THEORETICAL STUDY OF TUNNELING CONDUCTANCE IN NORMAL-METAL/INSULATOR/PrOs$_4$Sb$_{12}$ JUNCTIONS

SAEED BOHLOUL

Theoretical Study of Tunneling Conductance in Normal-Metal/Insulator/PrOs$_4$Sb$_{12}$ Junctions

by

©Saeed Bohloul

Abstract

Superconducting phase of $PrOs_4Sb_{12}$ is theoretically investigated by means of point contact Andreev reflection spectroscopy. The conductance spectrum of a normal-metal/insulator/$PrOs_4Sb_{12}$ junction is calculated by solving the three dimensional Bogoliubov–de Gennes equations. By using the phenomenological Landau theory, various order parameters are selected and examined as a candidate of superconductivity in $PrOs_4Sb_{12}$. These order parameters include both spin singlet and triplet channels.

The conductance spectrum of the junction show multiple features in both singlet and triplet channels including a peak in conductance at different energy points. In particular, a zero bias conductance peak (ZBCP) can be observed in some of the spectra which is a direct result of unconventional superconductivity. Comparison with experimental results indicate that superconductivity in $PrOs_4Sb_{12}$ is most likely caused by an order parameter in triplet channel. However, more experimental evidences are required in order to find the actual symmetry of superconducting phase in this material.

Acknowledgements

I would like to thank Dr. Stephanie Curnoe for providing me the opportunity to work on this project and helping me through each level of this research. I would also like to thank all the people who helped me and made my life possible during these two years in St. John's.

To

Ferdinand Bardamu

and thanks to my lovely

Mother

and

Father

Table of Contents

List of Tables

List of Figures

xi

Chapter 1

Introduction

Superconductivity has been one the most intriguing and fascinating phases of matter since its discovery [1]. Superconductors are best known for their zero electrical resistivity and perfect diamagnetism below a certain temperature which is referred as the critical temperature T_c . According to the theory proposed by Bardeen, Cooper and Schrieffer[1] in 1957, superconductivity is a condensate of electron pairs which are called Cooper pairs. The formation of these pairs is due to an attractive interaction between the electrons. In early discovered superconductors, electron-phonon coupling mediates this interaction. This leads to the formation of the most symmetric Cooper pairs with vanishing relative orbital angular momentum and a singlet spin configuration. This kind of pairing is known as s-wave pairing since it is characterized by $L = 0$, where L is the orbital angular momentum. Conventional superconductors are those with s-wave pairing.

Unconventional superconductors are those with $L \neq 0$ [2]. In this type of superconductor, the attractive interaction required for pair formation may originate from other

[1]the BCS theory [1]

1

sources such as magnetic interactions. In some superconductors, the Cooper pairs are in a spin triplet state, i.e. pairing with spin $S = 1$.

In general, the spin and momentum structure of the Cooper pairs is contained in the "gap function" [2]. This function is also known as the superconducting order parameter, and has a direct relation to the pair wave function. In the case of singlet pairing, the gap function can be characterized by a single complex function $\psi(\mathbf{k})$. For triplet pairing, due to three-fold degeneracy of spin state, the gap function is characterized by a vector function, $\mathbf{d}(\mathbf{k})$. The Pauli principle requires that $\psi(\mathbf{k})$ be an even function of $\mathbf{k}$, while $\mathbf{d}(\mathbf{k})$ is odd.

The anisotropic structure of superconducting gap in unconventional superconductors is the origin of many interesting features. These features such as high critical temperature and multiple transitions are not observed in conventional superconductors. Hence, understanding the structure of the superconducting gap function and studying the superconducting mechanism in unconventional superconductors is the subject of many of ongoing works.

New improvements in materials science leads to the discovery of new superconducting materials. Experimental and theoretical studies on these materials increase our knowledge about superconductivity phenomena and reveals the ways that this knowledge can be enhanced. Among various families of superconductors, the filled skutterudite family [3] is one of the newly discovered examples with interesting superconducting behaviors. In particular, superconductivity in $PrOs_4Sb_{12}$, which is known as the first heavy-fermion superconductor with Pr atoms, has become the topic of many experimental studies. Unlike other heavy-fermion superconductors, these atoms have no

magnetic moment [4].

Different studies indicate various unconventional properties for $PrOs_4Sb_{12}$ [5] which include the appearance of two superconducting transition temperatures [6, 7, 8, 9]. These transitions occur at $T_{c1} = 1.85$ K (phase A) and $T_{c2} = 1.75$ K (phase B). Based on these observations, $PrOs_4Sb_{12}$ is expected to have an unusual pairing mechanism. In addition, by using angular magneto-thermal conductivity measurements, it is shown that the pairing symmetry of $PrOs_4Sb_{12}$ experiences a phase transition in a magnetic field [10].

Experimental reports regarding the topology of the superconducting gap in $PrOs_4Sb_{12}$ are not consistent. Some of these experiments predict the presence of nodes in the gap function while others indicate that it is fully gapped [11]. It has even been suggested that the observed double superconducting transitions, is a result of a non-nodal superconducting gap together with nodal one [12].

Strong evidence confirming the double transitions scenario can be provided by thermal conductivity measurements [13, 14]. The provided data shows that $PrOs_4Sb_{12}$ is very likely to be an unconventional superconductor, having two transition temperatures. In fact, small values measured in $PrOs_4Sb_{12}$ for residual electronic conductivity divided by the temperature, κ_0/T, indicate the presence of nodes in the superconducting gap function. On the other hand, measuring the thermal conductivity in an external magnetic field shows a rapid growth of thermal conductance at low temperatures. This behavior corresponds to a non-nodal superconducting gap, in contrast with exponential growth of conductivity in the case of a nodal gap.

Despite all these experimental efforts, the symmetry of the superconducting order parameter is still a central issue in studying superconductivity in $PrOs_4Sb_{12}$. However, a large number of these experiments are known as bulk probes which are not appropriate to directly detect the gap inhomogeneity. On the other hand, point-contact Andreev reflection spectroscopy (PCARS), is a method of investigating the symmetry of the superconducting which can be exploited to study local properties of materials. Hence, it is sensitive to the phase of superconducting order parameter [15].

Theoretical PCARS studies of $PrOs_4Sb_{12}$ along with the experimental results, provide useful information regarding the symmetry of the order parameter in this material. In particular, in cases where there is little or no information about the mechanism of superconductivity, the phenomenological Landau theory approach [39] is an ideal tool to describe the superconducting phase of materials. This approach provides us with all the possible symmetry properties of the superconducting state only by knowing the crystal point group symmetry. All the order parameters are classified using this symmetry group.

Experiments show that the point group of $PrOs_4Sb_{12}$ is tetrahedral, (T_h). Therefore using a Landau theory approach, the superconducting states of this material can be classified as given in Table 1 [3].

In the following chapters, we study PCARS of normal-metal/insulator/$PrOs_4Sb_{12}$ junctions by following the formalism invented by Blonder, Tinkham and Klapwijk (BTK) [21]. In Chapter 2 and Chapter 3 we will develop the required theoretical tools and in Chapter 4 and Chapter 5 we will report the results of our calculation for a number of states included in Table 1. We use this to show which of these states are

	State	Symmetry
1D order parameter	(1)	$T \times K$
2D order parameter	$(1,0)$	$T(D_2)$
	(ϕ_1, ϕ_2)	$D_2 \times K$
	(η_1, η_2)	D_2
3D order parameter	$(1,0,0)$	$D_2(C_2) \times K$
	$(1,1,1)$	$C_3 \times K$
	$(1, \epsilon, \epsilon^2)$	$C_3(E)$
	$(|\eta_1|, i|\eta_2|, 0)$	$D_2(E)$
	$(|\eta_1|, |\eta_2|, 0)$	$C_2(E) \times K$
	$(\eta_1, \eta_2, 0)$	$C_2(E)$
	$(\eta_1, i|\eta_2|, |\eta_3|)$	$C_2'(E)$
	$(|\eta_1|, |\eta_2|, |\eta_3|)$	K
	(η_1, η_2, η_3)	E

Table 1.1: Superconducting states of the point group T_h obtained by one irreducible representation. The third column shows the symmetry group of the superconducting states [3] .

real physical candidates of superconductivity in $PrOs_4Sb_{12}$ [3].

Chapter 2

Point-Contact Andreev Reflection Spectroscopy

Point-contact spectroscopy (PCS) is an experimental tool for investigating the interaction mechanisms between electrons and different elementary excitations in solid state materials [16]. In general, the $I - V$ characteristic (and second derivative d^2V/dI^2) of small micro-constrictions between two materials include some nonlinearities which are related to different quantum processes that electrons undergo in their interactions with elementary excitations. Analyzing these deviations in the $I - V$ curve provides a way to find information on the nature of these interactions. Depending on the materials used on each side of the contact, different quantum phenomena occur at the interface. When a superconductor is used in one side of the point-contact (which is the main topic of this work), it is known as point-contact Andreev reflection spectroscopy (PCARS) [15] because quantum phenomena, such as quasi-particle tunneling and Andreev reflection [17], dominate the physical processes that occur at the interface. This type of point-contact helps to find fundamental information on the excitation spectrum of the quasi-particles, in other words, on the superconducting energy gap

and its properties. In general, these physical phenomena are affected by the regimes of conduction in the contact. Understanding these regimes may help in better understanding the theoretical and experimental aspects of point-contact spectroscopy in normal metals and superconductors.

2.1 Regimes of the conduction in a point-contact

The radius of the point-contact, which is simply a contact between two materials (normal-metal and superconductor in this work), characterizes the regime of conductance in a point-contact spectroscopy experiment. Depending on the size of the contact a in comparison to the electron mean free path l, three different regimes of conductance are possible, as explained in the following.

2.1.1 Ballistic regime

In this regime, the electron mean free path l is much larger than the contact radius a ($l \gg a$). By applying voltage V to the contact, the electrons will be accelerated within the distance of a mean free path. These electrons experience no scattering and flow through the contact ballistically. In this case, their kinetic energy is equal to eV. (see Figure 2.1). The resistance of the contact in this regime is equal to

$$R_S = \frac{4\rho l}{3\pi a^2} \tag{2.1}$$

which was calculated by Sharvin [18]. In this equation ρ indicates the resistivity of the contact material. Considering the fact that in metals $\rho \propto l^{-1}$, R_S can be written in the following form, in the free electron approximation
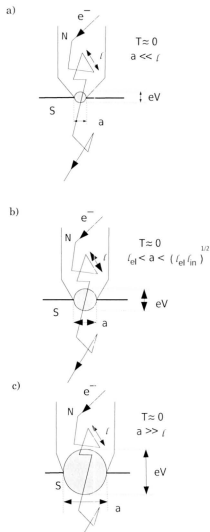
Figure 2.1: Schematic illustration of different conduction regimes in a point contact [24] where N and S represent normal-metal and superconductor respectively. (a) Ballistic regime with no scattering. (b) Diffusive regime in which only elastic scattering occurs in the contact. (c) Thermal regime with inelastic scattering.

$$R_S = \frac{2\hbar}{c^2 k_F^2 a^2} \tag{2.2}$$

where k_F is the Fermi momentum of the material [19]. Therefore in the ballistic regime, the energy of the electron is known and related to the applied voltage.

2.1.2 Thermal regime

This regime is the opposite case of the ballistic regime in which $l \ll a$ (see Figure 2.1). In the thermal (also called Maxwell) regime, electrons can undergo both elastic and inelastic scattering in the contact region. This is similar to the behavior of electrons in bulk. The resistance of the junction is determined by

$$R_M = \frac{\rho}{2a} \tag{2.3}$$

which was already calculated by Maxwell [20]. In this equation ρ shows the resistivity of the metal. Due to Joule heating, the local temperature of the contact increases such that the maximum temperature of the contact can be estimated by [20]

$$T_{max}^2 = T_{bath}^2 + \frac{V^2}{4L} \tag{2.4}$$

where T_{bath} indicates bath temperature and L is the Lorentz number whose value is roughly $2.45 \times 10^{-8} V^2/K^2$. Since the resistivity of metals ρ becomes greater with temperature, the conductance of the contact decreases with bias and any information on the inelastic scattering of the electrons is lost. Therefore, energy resolved spectroscopy is not possible in the thermal regime.

2.1.3 Diffusive regime

It is also possible to define another regime between the thermal and ballistic regime in which $l_{el} < a < l_{in}$. Accordingly, the quasi-particles inside the contact region can undergo elastic scattering but not an inelastic one. Therefore, because of elastic scattering, these particles lose the momentum information while the energy information is retained due to lack of inelastic scattering. Hence, in the diffusive regime only energy resolved spectroscopy can be performed with a point-contact.

In general, only the ballistic regime provides a way to perform both energy and momentum resolved spectroscopy with point-contacts. In the rest of this work, we always consider a point-contact in the ballistic regime. Therefore, the whole voltage drop for the particles occurs at the interface.

2.2 Physics of the interface in a point contact

2.2.1 Andreev reflection

In the case of a normal-metal/superconductor contact, the electrical transport through the contact is dominated by a process called *Andreev* reflection which was first predicted by Andreev [17]. This process is illustrated in Figure 2.3 in which a normal metal (N) is brought in direct contact with a superconductor (S). Working in the ballistic regime, an electron coming from the N side accelerates in applied voltage V and gains an energy equal to eV. If this energy is less than the superconducting energy gap in the S side, Δ, then electrons can not propagate through the interface. This happens because only the Cooper pair exists in this energy range in S and the electron is unable to form a pair with an energy less than the superconducting energy

Figure 2.2: Ordinary specular reflection (left hand side) and Andreev reflection (right hand side). The group velocity of the incoming and outgoing particles is shown by the arrows. In the case of the Andreev reflection, the outgoing particle traces back the trajectory of the incoming particle which is called retro-reflection.

gap $eV < \Delta$. In this case, the incident electron is reflected back inside the normal metal as a hole, and two electrons transmitted in the superconductor as a Cooper pair, such that the total charge and momentum is conserved. If we consider a singlet spin Cooper pair in the S side, the reflected hole propagates in the opposite spin band to that of the incident electron with opposite wave vector. This phenomenon is called retro-reflection, in which the hole traces back the trajectory of the incoming electron (see Figure 2.2).

On the other hand, if $eV > \Delta$, then the incoming electron can propagate to the S side and form a Cooper pair. This pair is the source of the super current in the superconductor. However, there are still electrons with energy less than the superconducting energy gap, which may undergo Andreev reflection. There is also another possibility in which the incoming electron is reflected normally as an electron at the interface. This phenomenon is called specular reflection (see Figure 2.2).

Due to Andreev reflection, the conductance of the junction becomes double for $eV < \Delta$. This provides useful information on the energy gap in the S side which is the main application of PCARS. In general, the state of the quasi-particles at the interface of the N/S junction is described by the solution of the Bogoliubov-de Gennes (BdG) equations [19]. From these equations, one can conclude that Andreev reflection does not occur abruptly at the interface. In fact, it happens over a length scale of the order ξ. This length is the same as the superconductivity coherence length over which Δ is depressed because of the proximity effect generated by N on S. For contact sizes smaller than ξ this effect can be neglected.

Therefore, it is necessary to use contacts which are smaller than the electron mean free path $(a < l)$ and the coherence length $(a < \xi)$ to avoid the heating and proximity effects respectively.

2.2.2 The Blonder, Tinkham and Klapwijk (BTK) formalism

Although Andreev reflection was discovered in the early 1960s, it took almost 20 years to develop a framework for analyzing the PCARS spectrum. This work was done by Blonder, Tinkham and Klapwijk [21] which is known as the BTK theory. In this model, the state of the quasi-particles at the N/S interface can be described by the BdG equations. The barrier at the interface is shown by a repulsive potential and all of the system is considered to be one dimensional. In the following, the details of this theory are explained.

2.2.2.1 Bogoliubov-de Gennes equations

The BdG equations provide an appropriate method for analyzing quasi-particle spectra in superconductors. In particular, the state of quasi-particles is described by two

functions u and v (considering particles without spin) [19]

$$\epsilon \left(\begin{array}{c} u_{\mathbf{k}}(\mathbf{r}) \\ v_{\mathbf{k}}(\mathbf{r}) \end{array} \right) = \left(\begin{array}{cc} \hat{H}(\mathbf{k}, \mathbf{r}) & \hat{\Delta}(\mathbf{k}, \mathbf{r}) \\ \hat{\Delta}^{\star}(\mathbf{k}, \mathbf{r}) & -\hat{H}^{\star}(\mathbf{k}, \mathbf{r}) \end{array} \right) \left(\begin{array}{c} u_{\mathbf{k}}(\mathbf{r}) \\ v_{\mathbf{k}}(\mathbf{r}) \end{array} \right) \quad (2.5)$$

where $\hat{H} = \frac{1}{2m}(\mathbf{p} - \frac{e}{c}\mathbf{A})^2 + V - E_F$. In this equation, $\mathbf{A}$ and V represent external magnetic and electric potential respectively, and E_F is the Fermi energy of the material under consideration. Also ϵ is the energy of quasi-particles measured from the Fermi energy and $\hat{\Delta}$ shows the superconducting pairing potential, which is a function of position $\mathbf{r}$ and momentum $\mathbf{k}$ in general. In case of metals where $\hat{\Delta}$ vanishes, these u and v functions describe state of independent electrons and holes, while in a superconductor with non-zero $\hat{\Delta}$, we deal with a mixture of hole and electron excitations.

Following the BTK formalism, if we consider a one dimensional interface located in the xy plane at $z = 0$, all the momenta in the problem are normal to the interface and thus parallel to the z axis. We also assume that interface is described by a repulsive delta potential $H\delta(z)$. In the case of conventional superconductors with $\hat{\Delta}(\mathbf{k}, \mathbf{r}) = \Delta_0$, the BdG equations at the normal-metal/superconductor (N/S) interface are reduced to

$$Eu(z) = h(z)u(z) + \Delta_0 \Theta(z) v(z) \quad (2.6)$$

$$Ev(z) = -h(z)v(z) + \Delta_0^{\star}\Theta(z)u(z) \quad (2.7)$$

where $h(z) = -\frac{\hbar^2}{2m}\frac{d^2}{dz^2} - E_F + U(z)$, $\Theta(z)$ is the Heaviside step function and E is the energy of the injected particles.

2.2.2.2 BTK coefficients

According to the BTK model, which is based on zero temperature calculations, the injected electron from the normal side to the superconductor may undergo different processes depending on the energy E, as shown in Figure 2.3. The probability of these processes can be obtained by solving the aforementioned BdG equations and using appropriate boundary conditions. When the electron approaches the interface with E larger than the pair potential amplitude ($E > |\Delta_0|$), it advances in four trajectories:

1. The electron can be reflected as an electron whose momentum component normal to the interface is reversed and the two other momentum components are conserved because of the translational symmetry at the interface, i.e. it propagates with $(k_x, k_y, -k_z)$ assuming that (k_x, k_y, k_z) represents the wave vector of the incident electron. The probability of this process is denoted by B.

2. The electron can also be reflected as a hole (Andreev reflection). In this case, the hole propagates in the metal with a wave vector exactly opposite to that of the electron, i.e. $(-k_x, -k_y, -k_z)$ which is called retro-reflection. The probability of this process is denoted by A.

3. The electron can be transmitted to the superconductor as an electron-like quasi-particle (ELQ) whose probability is denoted by C.

4. The electron can be transmitted to the superconductor as a hole-like quasi-particle (HLQ) whose probability is denoted by D.

In the case of Andreev reflection, the injected electron forms a Cooper pair with another electron near the Fermi surface of the superconductor. This electron should have a wavevector inverse to that of the first electron. Hence the vacant place of this electron propagates with the inverse wavevector, which is equivalent to the emission

of a hole.

On the other hand, when energy of the injected electron is less than the pair potential amplitude ($E < |\Delta_0|$), the transmission of the electron as ELQ and HLQ is forbidden and the current is carried by Cooper pairs (see Figure 2.3). Obviously, the existence of the pair potential causes the Andreev reflection process.

2.2.2.3   Solution of the BdG equations for one dimensional junction

As already mentioned, the probability amplitude of each process (A,B,C,D) can be found by solving Equations (2.6) and (2.7) following the appropriate boundary conditions. These equations are similar to the ordinary Schrödinger equation in the case of a δ potential where the wave-functions in the N and S sides are forced to match at $z = 0$ with boundary potential $H\delta(z)$. Therefore, the wave function on the normal side is the sum of the wave functions of the possible processes explained in the previous section multiplied by their amplitudes. Considering ψ_N as the wave function on the N side then we have

$$\psi_N(z) = \psi_{inc}(z) + A\psi_a(z) + B\psi_b(z) \qquad (2.8)$$

where ψ_{inc} is the wave function of the incoming particle and ψ_a and ψ_b represents the wave functions of Andreev and specular reflection respectively. On the superconductor side, the superposition of the quasi-particle wave functions is given by

$$\psi_S(z) = C\psi_c(z) + D\psi_d(z) \qquad (2.9)$$

Here, ψ_c and ψ_d describe the state of electron-like and hole-like quasi-particles respectively.
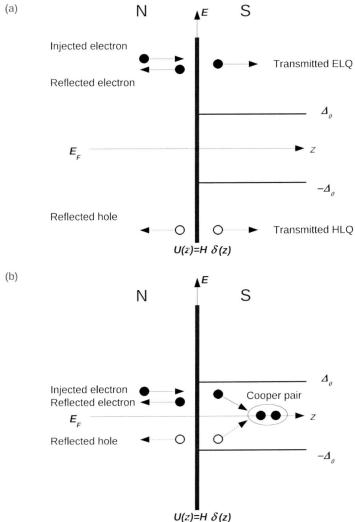
Figure 2.3: Schematic illustration of electron injection in a normal-metal/superconductor junction. The electron is injected with energy E. Open circles represent hole (-like quasi-particle) while closed circles show electron (-like quasi-particle). For $E > |\Delta_0|$ (a) the electron (hole) is normally transmitted as an ELQ (HLQ). For $E < |\Delta_0|$ (b), the presence of the ELQ (HLQ) is forbidden in the superconductor. Hence, the current is carried by formation of a Cooper pair.

If we assume injected electrons with wave vector k_N^+, then the wave functions of the particles propagating on the normal side can be written as

$$
\begin{aligned}
\psi_{inc} &= \begin{pmatrix} 1 \\ 0 \end{pmatrix} e^{ik_N^+ z} \\
\psi_a &= \begin{pmatrix} 0 \\ 1 \end{pmatrix} e^{ik_N^- z} \\
\psi_b &= \begin{pmatrix} 1 \\ 0 \end{pmatrix} e^{-ik_N^+ z}.
\end{aligned}
\tag{2.10}
$$

The first function shows an electron moving in the positive z direction with wave vector k_N^+ while the last one represents an electron moving in the negative z direction with wave vector k_N^+. The second function is related to the motion of a hole toward the positive z with wave vector k_N^-.

For the S side these wave functions include BCS[1] coherence factors (see Appendix A) and are expressed in the following form

$$
\begin{aligned}
\psi_c &= \begin{pmatrix} u \\ ve^{-i\phi} \end{pmatrix} e^{ik_S^+ z} \\
\psi_d &= \begin{pmatrix} v \\ ue^{-i\phi} \end{pmatrix} e^{-ik_S^- z}.
\end{aligned}
\tag{2.11}
$$

---

[1]These factors describe the state of the Cooper pairs in a superconductor and are a result of the Bardeen, Cooper, and Schrieffer (BCS) theory of superconductivity.

where u and v are written as

$$u = \sqrt{\frac{E + \Omega}{2E}}$$
$$v = \sqrt{\frac{E - \Omega}{2E}} \qquad (2.12)$$
$$\Omega = \sqrt{E^2 - |\Delta_0|^2}$$

in which we consider E as the energy of the injected particle. Using these wave functions, the state of the system is written as

$$\Psi(z) = \begin{pmatrix} u(z) \\ v(z) \end{pmatrix} = \begin{cases} e^{ik_N^+ z} \begin{pmatrix} 1 \\ 0 \end{pmatrix} + A(E)e^{ik_N^- z} \begin{pmatrix} 0 \\ 1 \end{pmatrix} + B(E)e^{-ik_N^+ z} \begin{pmatrix} 1 \\ 0 \end{pmatrix} & z < 0 \\ C(E)e^{ik_S^+ z} \begin{pmatrix} u \\ v e^{-i\phi} \end{pmatrix} + D(E)e^{-ik_S^- z} \begin{pmatrix} v \\ u e^{-i\phi} \end{pmatrix} & z \geq 0 \end{cases} \qquad (2.13)$$

The wavefunction is continuous everywhere, in particular it is continuous at $z = 0$; but its first derivative has a discontinuity because there is a δ-function potential at $z = 0$. Therefore the matching conditions of the wavefunction are:

$$\Psi(z)|_{z=0+} = \Psi(z)|_{z=0-} \qquad (2.14)$$

$$\frac{d}{dz}\Psi(z)|_{z=0+} - \frac{d}{dz}\Psi(z)|_{z=0-} = \frac{2mH}{\hbar^2}\Psi(z)|_{z=0-} \qquad (2.15)$$

which can be used together with BdG equations to find eight unknowns k_N^+, k_N^-, k_S^+, k_S^-, $A(E)$, $B(E)$, $C(E)$, $D(E)$.

Substituting (2.13) into (2.6) and (2.7) results in

$$E\left[e^{ik_N^+z} + B(E)e^{-ik_N^+z}\right] = -\frac{\hbar^2}{2m}\left[(ik_N^+)^2e^{ik_N^+z} + (-ik_N^+)^2B(E)e^{-ik_N^+z}\right]$$
$$- E_F\left[e^{ik_N^+z} + B(E)e^{-ik_N^+z}\right]$$
$$EA(E)e^{ik_N^+z} = \frac{\hbar^2}{2m}(ik_N^-)^2A(E)e^{ik_N^-z} + E_FA(E)e^{ik_N^-z} \quad (2.16)$$

for $x < 0$ and

$$E\left[C(E)ue^{ik_S^+z} + D(E)ve^{-ik_S^-z}\right] =$$
$$- \frac{\hbar^2}{2m}\left[(ik_S^+)^2C(E)ue^{ik_S^+z} + (-ik_S^-)^2D(E)ve^{-ik_S^-z}\right]$$
$$- E_F\left[C(E)ue^{ik_S^+z} + D(E)ve^{-ik_S^-z}\right] + \Delta_0\left[C(E)ve^{-i\phi}e^{ik_S^+z} + D(E)ue^{-i\phi}e^{-ik_S^-z}\right]$$
$$E\left[C(E)ve^{-i\phi}e^{ik_S^+z} + D(E)ue^{-ik_S^-z}\right] =$$
$$\frac{\hbar^2}{2m}\left[(ik_S^+)^2C(E)ve^{-i\phi}e^{ik_S^+z} + (-ik_S^-)^2D(E)ue^{-ik_S^-z}\right]$$
$$+ E_F\left[C(E)ve^{-i\phi}e^{ik_S^+z} + D(E)ue^{-i\phi}e^{-ik_S^-z}\right] + \Delta_0^\star\left[C(E)ue^{ik_S^+z} + D(E)ve^{-ik_S^-z}\right]$$
$$(2.17)$$

for $x \geq 0$. In addition, the boundary conditions yield the following equations

$$1 + B(E) = C(E)u + D(E)v \quad (2.18)$$

$$A(E) = C(E)ve^{-i\phi} + D(E)ue^{-i\phi} \quad (2.19)$$

$$\left[(ik_S^+)C(E)u + (-ik_S^-)D(E)v\right] - \left[(ik_N^+) + B(E)(-ik_N^+)\right] = \frac{2mH}{\hbar^2}\left[1 + B(E)\right] \quad (2.20)$$

$$\left[(ik_S^+)C(E)ve^{-i\phi} + (-ik_S^-)D(E)ue^{-i\phi}\right] - \left[A(E)(ik_N^-)\right] = \frac{2mH}{\hbar^2}\left[A(E)\right] \quad (2.21)$$

Equations (2.16) and (2.17) can be simplified as

$$E = -\frac{\hbar^2}{2m}(ik_N^+)^2 - E_F$$

$$E = \frac{\hbar^2}{2m}(ik_N^-)^2 + E_F$$

$$Eu = -\frac{\hbar^2}{2m}(ik_S^+)^2 u - E_F u + \Delta_0 v e^{-i\phi}$$

$$Ev = -\frac{\hbar^2}{2m}(-ik_S^-)^2 v - E_F v + \Delta_0 u e^{-i\phi}$$

$$Eve^{-i\phi} = \frac{\hbar^2}{2m}(ik_S^+)^2 v e^{-i\phi} + E_F v e^{-i\phi} + \Delta_0^* u$$

$$Eue^{-i\phi} = \frac{\hbar^2}{2m}(-ik_S^-)^2 u e^{-i\phi} + E_F u e^{-i\phi} + \Delta_0^* v.$$

$$(2.22)$$

Using these equations, one can find for the wave vectors

$$\hbar k_N^\pm = \sqrt{2m(E_F \pm E)}$$

$$\hbar k_S^\pm = \sqrt{2m(E_F \pm \Omega)}$$

$$\Omega = \sqrt{E^2 - |\Delta_0|^2}.$$

$$(2.23)$$

The amplitude of the different processes at the interface are also obtained as

$$A(E) = \frac{uve^{-i\phi}}{(1+Z^2)u^2 - Z^2 v^2}$$

$$B(E) = \frac{Z(i+Z)(v^2 - u^2)}{(1+Z^2)u^2 - Z^2 v^2}$$

$$C(E) = \frac{(1-iZ)u}{(1+Z^2)u^2 - Z^2 v^2}$$

$$D(E) = \frac{iZv}{(1+Z^2)u^2 - Z^2 v^2}$$

$$(2.24)$$

where $Z = \frac{mH}{\hbar^2 k_F}$. Finding these unknowns enables us to calculate the conductance spectrum of the junction in terms of the energy of the injected particle, i.e. the bias voltage.

2.2.2.4 Normalized conductance

PCARS is considered as one of the highest-energy resolution probes of the electronic states. The amplitude of the current flow (I) depends on the bias voltage (V) which reflects the electronic structure of materials used on both sides of the contact. The essential concept of the BTK theory is to express the conductance of the junction by means of the reflection amplitude for electron injection. This approach is quite similar to Landauer's formula [22], which is useful for contacts made of normal metals. In this formulation, the electrons are randomly injected from a implicitly assumed thermal equilibrium heat bath. If we consider no scattering interaction in the junction area, then the conductance of a single channel is quantized in units of $2e/\hbar^2$ [23]. In the presence of scattering interactions, the transmission probability amplitude is different than one, hence the net current per channel is decreased.

In the BTK method, one of the electrodes is replaced by a superconductor, which results in the incorporation of Andreev reflection probability into the formula [21]. Consequently, net current associated with the Andreev reflection process affects the conductance spectrum in a serious way. Once the reflection coefficients of the BTK theory are found, it is possible to calculate the conductance spectrum of the N/S junction by

$$\sigma_S(E) = 1 + |A(E)|^2 - |B(E)|^2 \tag{2.25}$$

where the factor $2e/\hbar^2$ is neglected for simplicity. Although $\sigma_S(E)$ is written in terms of A and B, the contribution of C and D is already included in the calculations. This equation can easily be interpreted in terms of the charge flow conservation. If the injected electron is reflected as another electron, there is no contribution to net current flow. On the other hand, in case of Andreev reflection the reflected hole

increases the net current flow through the barrier, which is twice the probability amplitude of the Andreev reflection process. Dividing $\sigma_S(E)$ by the conductance of the junction when it is in normal state (σ_N) gives the normalized conductance which is the outcome of the PCARS experiment [21, 22]

$$\sigma(E) = \frac{\sigma_S(E)}{\sigma_N}. \tag{2.26}$$

Using the reflection coefficients in equation (2.24), $\sigma(E)$ is given by

$$\sigma(E) = \frac{1 + \sigma_N |\Gamma|^2 + (\sigma_N - 1)|\Gamma|^4}{|1 + (\sigma_N - 1)\Gamma^2|^2} \tag{2.27}$$

where

$$\sigma_N = \frac{1}{1 + Z^2} \tag{2.28}$$

and

$$\Gamma = \frac{|\Delta_0|}{E + \Omega}. \tag{2.29}$$

In the next section, the conductance spectrum of a junction for various values of Z is calculated, ranging from a perfectly transparent junction $Z = 0$ to $Z \to \infty$.

2.3   Conductance spectrum of one dimensional junction

In this Section, we consider a conventional superconductor with $\hat{\Delta} = \Delta_0$ for the S side of the junction. Equation (2.27) enables us to calculate the conductance spectrum of such a junction. In the actual experiment, the bias voltage, which forms the x-axis of the spectrum, is normalized to the largest value of the gap function (Δ_0 in this section). In fact, all the spectroscopic information on the superconducting state is
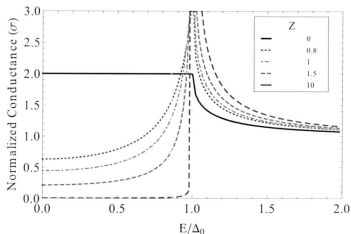
Figure 2.4: Normalized conductance spectra σ of a normal-metal/conventional super-conductor junction at $T = 0$ as a function of Z.

extracted from σ vs. x graph where x stands for $E/|\Delta_0|$. As already mentioned, E is the energy of injected electrons which depends on the applied voltage to the junction $E = eV$. Multiplying and dividing Γ in (2.29) by $|\Delta_0|$ results in

$$\Gamma = \frac{1}{x + \sqrt{x^2 - 1}}. \tag{2.30}$$

Therefore, the conductance in terms of the new parameter x is given by

$$\sigma(x, Z) = \frac{1 + \sigma_N |\frac{1}{x+\sqrt{x^2-1}}|^2 + (\sigma_N - 1)|\frac{1}{x+\sqrt{x^2-1}}|^4}{|1 + (\sigma_N - 1)(\frac{1}{x+\sqrt{x^2-1}})^2|^2}. \tag{2.31}$$

As can be seen from this equation, the normalized conductance is a function of Z (in addition to x) which represents the characteristics of the interface.

Figure 2.4 shows the normalized conductance spectrum of a one dimensional normal-

metal/conventional superconductor junction for various Z values. In the case of a perfectly transparent junction, where $Z = 0$, the conductance for $\frac{E}{|\Delta_0|} \leqslant 1$ is doubled with respect to the conductance in the normal state (σ_N). In this regime, which is called the pure Andreev regime, Andreev reflection takes place with probability 1. According to (2.24), for $Z = 0$, B is zero and A is given by

$$A(E) = \frac{v e^{-i\phi}}{u} \tag{2.32}$$

from which it can simply be understood that

$$
\begin{aligned}
|A(E)|^2 &= 1 \\
\sigma(x, 0) &= 2
\end{aligned}
\tag{2.33}
$$

With increasing Z, peak structures appear in the spectrum at $\frac{E}{|\Delta_0|} \approx 1$. As can be seen from Figure 2.4, the amplitude of the peaks increase on increasing Z. For larger Z values, the normalized conductance takes the form of the BCS quasi-particle density of states [24].

The BTK model can reproduce all the different experimental situations which arise from different transparencies at the N/S interface by introducing a simple parameter (Z). This parameter can range from zero to infinity. In particular, (2.27) enables us to extend the simple BTK formalism to two and three dimensional problems with more complexity. However, it should be noted that the original BTK model is derived by considering a large number of approximations and simplifications which can be listed as [24]

1. All the calculations are performed at zero temperature ($T = 0$).

2. The problem is limited to one dimension, such that all the injected particles are

perpendicular to the plane interface.

3. The barrier is assumed to be ideal with no thickness.

4. We consider a spherical Fermi surface in both sides of the junction.

5. Fermi velocity is the same in the N and S sides.

6. The N/S interface is assumed to be atomically flat.

In the following chapter, we will extend the BTK model to more realistic conditions by relaxing most of these restrictions. This provides us with a way for the analysis of PCARS results corresponding to a variety of unconventional superconductors such as $PrOs_4Sb_{12}$, which is the main superconductor under study in this work.

Chapter 3

Beyond the BTK Model

In a real normal-metal/superconductor (N/S) junction, the current injection is not really perpendicular to the interface. In fact, charge carriers approach the interface of N/S junction in any direction. The only constraint on the $\mathbf{k}$ vector is that its components parallel to the interface are conserved due to translational symmetry at the interface. Because of this conservation rule, the injected particle can still undergo the same processes at the interface as of a one dimensional junction (see Figure 3.1) [22, 26]. On the N side the injected electron with momentum $\mathbf{k} = (k_x, k_y, k_z)$ might be reflected as a hole with opposite wave vector $(-\mathbf{k})$ or as an electron with opposite transverse component of the wave vector $(k_x, k_y, -k_z)$. On the S side the ELQ propagates in the same direction as the incident particle (considering the same Fermi velocity in both sides of the junction), i.e. with the wave vector $\mathbf{k}$ while the HLQ propagates with the wave vector $(-k_x, -k_y, k_z)$. Therefore the BTK model should be extended to at least two dimensions.

Extending the BTK model to more than one dimension is also necessary when one deals with pair potentials having anisotropy in $\mathbf{k}$-space or unconventional supercon-

ductors. Since PCARS is a local probe, the interaction of the injected particle with the superconducting pairing potential depends on the direction it approaches the interface. Depending on this direction, the particle interacts with different parts of the pairing potential which generally are not the same.

The BTK model can also be generalized to situations where the Fermi velocity on N side differs from that on the S side. Following the formulation by Bruder [25], we extend the BTK model to two-dimensional and three-dimensional systems in this chapter.

3.1 2D system with singlet pair potential

3.1.1 Scattering amplitude coefficients

Suppose the injected electron on the N side, has energy E with upper-right-going wave vector as can be seen in Figure 3.1. This electron makes an angle θ to the interface normal ($\hat{x}$) such that $-\pi/2 < \theta < \pi/2$. Suppose that the wave vector of this electron is given by $\mathbf{k}_N^+$. The components of this wave vector are

$$
\begin{aligned}
k_{Nx}^+ &= k_N^+ \cos\theta \\
k_{Ny}^+ &= k_N^+ \sin\theta
\end{aligned}
\tag{3.1}
$$

If the pair potential is singlet, then we can treat the problem without including spin in the equations, similarly to the conventional superconductor case. Therefore, there are four possible scattering processes at the interface for the injected electron. These four trajectories and their corresponding wave vectors are given as

1. Andreev reflection: $\mathbf{k}_N^-$
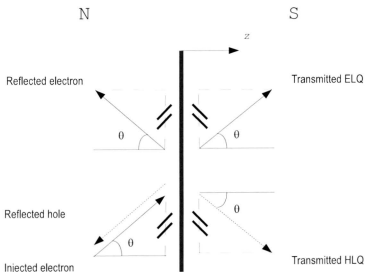
Figure 3.1: Schematic illustration of possible scattering processes at the interface of normal-metal/anisotropic superconductor. The electron is injected with angle θ to the interface normal (z-axis). Because of the assumed approximations, all trajectories have the same angle [22].

2. Normal reflection: $\mathbf{k}_N'^+$

3. ELQ: $\mathbf{k}_S^+$

4. HLQ: $\mathbf{k}_S^-$

Due to translational symmetry, the component of these wave vectors parallel to the interface (y-component) are all the same in magnitude. Therefore,

$$k_{Ny}^+ = |k_{Ny}'^+| = |k_{Ny}^-| = |k_{Sy}^+| = |k_{Sy}^-|. \tag{3.2}$$

The solution to the BTK coefficients can be obtained through the same steps as in Chapter 2 but it should be noted that the transmitted ELQ and HLQ interact with different effective pair potential. This happens because these particles propagate with different wave vectors, $\mathbf{k}_S^+$ and $\mathbf{k}_S^-$, respectively. Hence, the pair potential returns different values for these vectors in k-space ($\Delta = \Delta(\gamma)$ with $\gamma = \mathbf{k}/|\mathbf{k}|$),

$$\begin{aligned}
\Delta_+ &= \Delta(\gamma_+) = \Delta(\mathbf{k}_S^+/|\mathbf{k}_S^+|) \\
\Delta_- &= \Delta(\gamma_-) = \Delta(\mathbf{k}_S^-/|\mathbf{k}_S^-|).
\end{aligned} \tag{3.3}$$

Consequently, the BCS coherence factors, as a function of Δ, are different for ELQ and HLQ [27]. In addition, the phases of the effective pair potentials are given by

$$\begin{aligned}
\exp{(i\phi_+)} &\equiv \frac{\Delta_+}{|\Delta_+|} \\
\exp{(i\phi_-)} &\equiv \frac{\Delta_-}{|\Delta_-|}.
\end{aligned} \tag{3.4}$$

Using these equations, the wave function of the system can be written as

$$\Psi_N(\mathbf{r}) = e^{i\mathbf{k}_N^+ \cdot \mathbf{r}} \begin{pmatrix} 1 \\ 0 \end{pmatrix} + A(E)e^{i\mathbf{k}_N^- \cdot \mathbf{r}} \begin{pmatrix} 0 \\ 1 \end{pmatrix} + B(E)e^{-i\mathbf{k}_N^{\prime +} \cdot \mathbf{r}} \begin{pmatrix} 1 \\ 0 \end{pmatrix}$$

$$\Psi_S(\mathbf{r}) = C(E)e^{i\mathbf{k}_S^+ \cdot \mathbf{r}} \begin{pmatrix} u_+ \\ v_+ e^{-i\phi_+} \end{pmatrix} + D(E)e^{-i\mathbf{k}_S^- \cdot \mathbf{r}} \begin{pmatrix} v_- \\ u_- e^{-i\phi_-} \end{pmatrix}$$

(3.5)

where

$$u_\pm = \sqrt{(E + \Omega_\pm)/2E}$$

$$v_\pm = \sqrt{(E - \Omega_\pm)/2E}$$

(3.6)

$$\Omega_\pm = \sqrt{E^2 - |\Delta_\pm|^2}.$$

Substituting (3.5) in the BdG equations and applying the boundary conditions enables us to find the probability amplitude and the wave vectors. Because of translational symmetry at the interface and conservation of the momentum components along y-direction, only the x dependent part of the above equations participates in calculations. According to (3.2)

$$\mathbf{k}_N^- = (k_{Nx}^-, k_{Ny}^+)$$

$$\mathbf{k}_N^{\prime +} = (k_{Nx}^+, -k_{Ny}^+)$$

(3.7)

$$\mathbf{k}_S^+ = (k_{Sx}^+, k_{Ny}^+)$$

$$\mathbf{k}_S^- = (k_{Sx}^-, -k_{Ny}^+).$$

Therefore (3.5) is written as

$$\Psi_N(\mathbf{r}) = e^{ik_{Nx}^k x} e^{ik_{Ny}^k y} \begin{pmatrix} 1 \\ 0 \end{pmatrix} + A(E) e^{ik_{Nx}^k x} e^{ik_{Ny}^k y} \begin{pmatrix} 0 \\ 1 \end{pmatrix} + B(E) e^{-ik_{Nx}^k x} e^{ik_{Ny}^k y} \begin{pmatrix} 1 \\ 0 \end{pmatrix}$$

$$\Psi_S(\mathbf{r}) = C(E) e^{ik_{Sx}^k x} e^{ik_{Ny}^k y} \begin{pmatrix} u_+ \\ v_+ e^{-i\phi_+} \end{pmatrix} + D(E) e^{-ik_{Sx}^k x} e^{ik_{Ny}^k y} \begin{pmatrix} v_- \\ u_- e^{-i\phi_-} \end{pmatrix}.$$

$$(3.8)$$

Finally by factoring $e^{ik_{Ny}^k y}$, we find

$$\Psi_N(\mathbf{r}) = e^{ik_{Ny}^k y} \left[e^{ik_{Nx}^k x} \begin{pmatrix} 1 \\ 0 \end{pmatrix} + A(E) e^{ik_{Nx}^k x} \begin{pmatrix} 0 \\ 1 \end{pmatrix} + B(E) e^{-ik_{Nx}^k x} \begin{pmatrix} 1 \\ 0 \end{pmatrix} \right]$$

$$\Psi_S(\mathbf{r}) = e^{ik_{Ny}^k y} \left[C(E) e^{ik_{Sx}^k x} \begin{pmatrix} u_+ \\ v_+ e^{-i\phi_+} \end{pmatrix} + D(E) e^{-ik_{Sx}^k x} \begin{pmatrix} v_- \\ u_- e^{-i\phi_-} \end{pmatrix} \right].$$

$$(3.9)$$

Hence, boundary conditions are only applied in x-direction,

$$\Psi_N(\mathbf{r})|_{x=0-} = \Psi_S(\mathbf{r})|_{x=0+} \tag{3.10}$$

$$\frac{d\Psi_S(\mathbf{r})}{dx}\bigg|_{x=0+} - \frac{d\Psi_N(\mathbf{r})}{dx}\bigg|_{x=0-} = \frac{2mH}{\hbar^2} \Psi_S(\mathbf{r})|_{x=0+}. \tag{3.11}$$

From the BdG equations, one can find

$$E\left[e^{ik_{Nx}^+x} + B(E)e^{-ik_{Nx}^+x}\right] = -\frac{\hbar^2}{2m}\left[(ik_{Nx}^+)^2 e^{ik_{Nx}^+x} + (-ik_{Nx}^+)^2 B(E)e^{-ik_{Nx}^+x}\right]$$

$$- E_F\left[e^{ik_{Nx}^+x} + B(E)e^{-ik_{Nx}^+x}\right]$$

$$EA(E)e^{ik_{Nx}^-x} = \frac{\hbar^2}{2m}(ik_{Nx}^-)^2 A(E)e^{ik_{Nx}^-x} + E_F A(E)e^{ik_{Nx}^-x}$$

$$E\left[C(E)u_+ e^{ik_{Sx}^+x} + D(E)v_- e^{-ik_{Sx}^+x}\right] =$$

$$- \frac{\hbar^2}{2m}\left[(ik_{Sx}^+)^2 C(E)u_+ e^{ik_{Sx}^+x} + (-ik_{Sx}^+)^2 D(E)v_- e^{-ik_{Sx}^+x}\right]$$

$$- E_F\left[C(E)u_+ e^{ik_{Sx}^+x} + D(E)v_- e^{-ik_{Sx}^+x}\right] + \Delta\left[C(E)v_+ e^{-i\phi_+} e^{ik_{Sx}^+x} + D(E)u_- e^{-i\phi_-} e^{-ik_{Sx}^+x}\right]$$

$$E\left[C(E)v_+ e^{-i\phi_+} e^{ik_{Sx}^+x} + D(E)u_- e^{-i\phi_-} e^{-ik_{Sx}^+x}\right] =$$

$$\frac{\hbar^2}{2m}\left[(ik_{Sx}^+)^2 C(E)v_+ e^{-i\phi_+} e^{ik_{Sx}^+x} + (-ik_{Sx}^+)^2 D(E)u_- e^{-i\phi_-} e^{-ik_{Sx}^+x}\right]$$

$$+ E_F\left[C(E)v_+ e^{-i\phi_+} e^{ik_{Sx}^+x} + D(E)u_- e^{-i\phi_-} e^{-ik_{Sx}^+x}\right] + \Delta^*\left[C(E)u_+ e^{ik_{Sx}^+x} + D(E)v_- e^{-ik_{Sx}^+x}\right].$$

$$(3.12)$$

The boundary conditions yield

$$1 + B(E) = C(E)u_+ + D(E)v_- \tag{3.13}$$

$$A(E) = C(E)v_+ e^{-i\phi_+} + D(E)u_- e^{-i\phi_-} \tag{3.14}$$

$$\left[(ik_{Sx}^+)C(E)u_+ + (-ik_{Sx}^+)D(E)v_-\right] - \left[(ik_{Nx}^+) + B(E)(-ik_{Nx}^+)\right] = \frac{2mH}{\hbar^2}\left[1 + B(E)\right] \tag{3.15}$$

$$\left[(ik_{Sx}^+)C(E)v_+ e^{-i\phi_+} + (-ik_{Sx}^-)D(E)u_- e^{-i\phi_-}\right] - \left[A(E)(ik_{Nx}^-)\right] = \frac{2mH}{\hbar^2}\left[A(E)\right]. \tag{3.16}$$

By solving this set of equations the wave vectors and probability amplitude are found as

$$\hbar k_N^{\pm} = \sqrt{2m(E_F \pm i\varepsilon)}$$

$$\hbar k_S^{\pm} = \sqrt{2m(E_F \pm \Omega_{\pm})}$$

$$A(E, \theta) = \frac{\exp(-i\phi_{\pm})u_- v_+}{(1 + Z'^2)u_+ v_- - Z'^2 v_+ v_- \exp(i\phi_- - i\phi_+)}$$

$$B(E, \theta) = \frac{Z'(i + Z'[v_+ v_- \exp(i\phi_- - i\phi_+) - u_+ u_-])}{(1 + Z'^2)u_+ u_- - Z'^2 v_+ v_- \exp(i\phi_- - i\phi_+)} \quad (3.17)$$

$$C(E, \theta) = \frac{(1 - iZ')u_-}{(1 + Z'^2)u_+ u_- - Z'^2 v_+ v_- \exp(i\phi_- - i\phi_+)}$$

$$D(E, \theta) = \frac{\exp(i\phi_- - i\phi_+)iZ' v_+}{(1 + Z'^2)u_+ v_- - Z'^2 v_+ v_- \exp(i\phi_- - i\phi_+)}$$

where $Z' = \frac{mH}{\hbar^2 k_F \cos\theta}$. Assuming that $E_F \gg E, |\Delta(\mathbf{k})|$, the magnitude of all the wave vectors can be approximated by k_F,

$$\hbar k_N^{\pm} = \sqrt{2m(E_F \pm E)} \approx \hbar k_F.$$

$$\hbar k_S^{\pm} = \sqrt{2m(E_F \pm \Omega_{\pm})} \approx \hbar k_F. \quad (3.18)$$

As a result, all the particles make the same angle as the incident particle with the x-direction, i.e all the trajectories are defined by angle θ as shown in Figure 3.1.

$$k_{Nx}^+ \approx k_{Nx}^- \approx k_{Sx}^+ \approx k_{Sx}^- \approx k_F \cos\theta \quad (3.19)$$

Also, we already assumed that k_F is the same in both sides of the junction ($|\mathbf{k}_{FN}| = |\mathbf{k}_{FS}|$). Note that for a conventional superconductor ($\Delta_+ = \Delta_-$), we retrieve the BTK

result by putting $\theta = 0$ in (3.17),

$$u_+ = u_- = u$$
$$v_+ = v_- = v$$
$$\phi_+ = \phi_- = \phi$$
$$Z' = Z$$
$$A(E,0) = \frac{\exp(-i\phi)uv}{(1+Z^2)u^2 - Z^2v^2} = A(E)$$
$$B(E,0) = \frac{Z(i + Z[vv - uu])}{(1+Z^2)u^2 - Z^2v^2} = B(E)$$
$$C(E,0) = \frac{(1-iZ)u}{(1+Z^2)u^2 - Z^2v^2} = C(E)$$
$$D(E,0) = \frac{iZv}{(1+Z^2)u^2 - Z^2v^2} = D(E).$$

(3.20)

As it is expected from the Andreev theory [17], when there is no insulating barrier at the interface (i.e. $Z = 0$), the normal reflection coefficient $B(E,\theta)$ vanishes. In this situation, only Δ_+ contributes to Andreev reflection.

3.1.2 Conductance spectrum

Using the above coefficients, the angle-resolved and normal conductance for the electron injection with angle θ are given by [22]

$$\sigma_S(E,\theta) = \sigma_N \frac{1 + \sigma_N|\Gamma_+|^2 + (\sigma_N - 1)|\Gamma_+\Gamma_-|^2}{|1 + (\sigma_N - 1)\Gamma_+\Gamma_- \exp(i\phi_- - i\phi_+)|^2} \tag{3.21}$$

$$\sigma_N = \frac{1}{1 + Z'^2} \tag{3.22}$$

$$\Gamma_\pm = \frac{E - \Omega_\pm}{|\Delta_\pm|} \tag{3.23}$$

By setting $\Delta_+ = \Delta_-$, i.e. the case of conventional superconductor, (3.21) is reduced to the usual BTK formula. As can be seen, these equations are not symmetric with

respect to the exchange of the subscripts $+$ and $-$. Therefore, for injection angles θ and $-\theta$, the conductance spectrum looks different.

For a real N/S junction, the particles are injected from all angles ($-\pi/2 < \theta < +\pi/2$). Hence, since the injection is toward $-k_x$ in k-space, the normalized conductance spectrum $\sigma(E)$ can be obtained by the integration over the solid angle on the half-sphere of the Fermi surface:

$$\sigma(E) = \frac{\int \, d\omega \, \sigma_S(E, \theta)}{\int \, d\omega \, \sigma_N}. \tag{3.24}$$

The solid angle for a two-dimensional system is given by

$$d\omega = \cos\theta \, d\theta, \tag{3.25}$$

therefore (3.24) can be written as

$$\sigma(E) = \frac{\int_{-\pi/2}^{\pi/2} d\theta \, \cos\theta \, \sigma_S(E, \theta)}{\int_{-\pi/2}^{\pi/2} d\theta \, \cos\theta \, \sigma_N}. \tag{3.26}$$

In addition to the amplitude, the conductance spectrum is also sensitive to the phase of the pair potential. Therefore, studying the phase of the Cooper pairs in a superconductor is also possible by analyzing the normalized conductance spectrum of a N/S junction. In the next Section, we will analyze the conductance spectrum for a number of junctions with various symmetries for the superconductor.

3.1.3   Conductance spectrum of two dimensional junctions

In this section we analyze the conductance spectrum for the following cases

1. $\Delta_+ = \Delta_- = \Delta_0$

2. $\Delta_+ = -\Delta_- = \Delta_0$

3. $\Delta_+ \exp(i\pi/2) = -\Delta_- = \Delta_0$

In each case, σ is calculated for different Z values. It may be noted that these cases include differences in both the amplitude and phase of the pairing gap. Then we analyze high-T_c superconductor junctions which are two dimensional.

3.1.3.1 Case one: $\Delta_+ = \Delta_- = \Delta_0$

This case corresponds to an s-wave superconductor. Since the symmetry of the pair potential is isotropic, the conductance of the two dimensional junction looks exactly the same as the one dimensional junction. Using (3.21), we can write the conductance in terms of a new parameter x as,

$$\sigma_S(x,\theta) = \sigma_N \frac{1 + \sigma_N|\Gamma|^2 + (\sigma_N - 1)|\Gamma^2|^2}{|1 + (\sigma_N - 1)\Gamma^2|^2}$$

$$\Gamma = x - \sqrt{x^2 - 1}$$

(3.27)

where $x = E/|\Delta_0|$. The conductance spectrum for this case is shown in Figure 3.2.

3.1.3.2 Case two: $\Delta_+ = -\Delta_- = \Delta_0$

In this case, the phases of Δ_+ and Δ_- are different. The phase difference is π which causes the appearance of a peak at zero energy (see Figure 3.3). This peak is called a zero bias conductance peak (ZBCP). The conductance can be written as,

$$\sigma_S(x,\theta) = \sigma_N \frac{1 + \sigma_N|\Gamma_+|^2 + (\sigma_N - 1)|\Gamma_+\Gamma_-|^2}{|1 + (\sigma_N - 1)\Gamma_+\Gamma_- \exp(i\pi)|^2}$$

$$\Gamma_\pm = x - \sqrt{x^2 - 1}$$

(3.28)
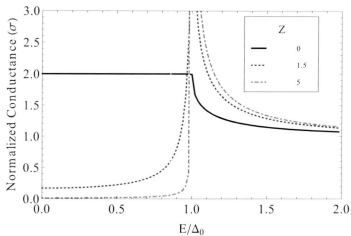
Figure 3.2: Conductance spectrum for a 2D junction with $\Delta_+ = \Delta_- = \Delta_0$.
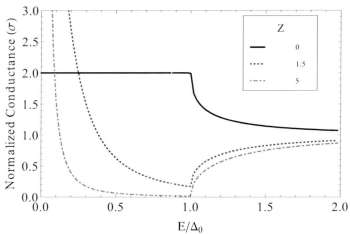
Figure 3.3: Conductance spectrum for a 2D junction with $\Delta_+ = -\Delta_- = \Delta_0$.
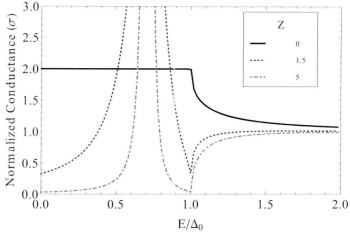
Figure 3.4: Conductance spectrum for a 2D junction with $\Delta_+ \exp(i\pi/2) = -\Delta_- = \Delta_0$.

3.1.3.3 Case three: $\Delta_+ \exp(i\pi/2) = -\Delta_- = \Delta_0$

In this case, the phase difference of Δ_- and Δ_- is $\pi/2$. The conductance can be written as

$$\sigma_S(x, \theta) = \sigma_N \frac{1 + \sigma_N |\Gamma_+|^2 + (\sigma_N - 1)|\Gamma_+ \Gamma_-|^2}{|1 + (\sigma_N - 1)\Gamma_+ \Gamma_- \exp(i\pi/2)|^2}$$

$$\Gamma_\pm = x - \sqrt{x^2 - 1}.$$

(3.29)

For this symmetry, a peak is observed at $E/\Delta_0 = \sqrt{2}/2$ (see Figure 3.4).

3.1.3.4 Junctions with high-T_c superconductors

When a junction is made of high-T_c superconductors, the effective pair potential is generally only a function of two components of the **k** vector. For example consider extended s wave, $s + id_{x^2-y^2}$ wave and $d_{x^2-y^2}$ superconductors. The functional forms

of these pair potentials are

$$\Delta(\mathbf{k}) = \Delta_1 + \Delta_2 \cos 4\theta_a \qquad (3.30)$$

$$\Delta(\mathbf{k}) = \Delta_1 + i\Delta_2 \cos 2\theta_a \qquad (3.31)$$

$$\Delta(\mathbf{k}) = \Delta_1 \cos 2\theta_a, \qquad (3.32)$$

respectively.

Here, θ_a represents the angle between a axis of the superconductor and the vector $(k_x, k_y, 0)$. (see Figure 3.5). Using the above formulation, the conductance of the junction can be calculated for different tunneling directions. In the case of two-dimensional superconductors, we can have c-axis tunneling and ab-plane tunneling.

For the c-axis tunneling, $\Delta_+ = \Delta_-$ regardless of the injection angle and symmetry of the pair potential. Figure 3.6 shows the conductance spectrum of c-axis tunneling for the above for the above pairings. Arbitrary values for the various parameters which appear in the order parameter were used.

On the other hand, when the tunneling direction is in ab-plane of the superconductor, $\Delta_+ = \Delta_-$ is not generally satisfied. Therefore, the conductance is expected to depend on α, the angle between the a axis and the interface normal. The pair potentials for the above symmetries in terms of α are

$$\Delta(\mathbf{k}) = \Delta_1 + \Delta_2 \cos 4(\theta - \alpha) \qquad (3.33)$$

$$\Delta(\mathbf{k}) = \Delta_1 + i\Delta_2 \cos 2(\theta - \alpha) \qquad (3.34)$$

$$\Delta(\mathbf{k}) = \Delta_1 \cos 2(\theta - \alpha) \qquad (3.35)$$
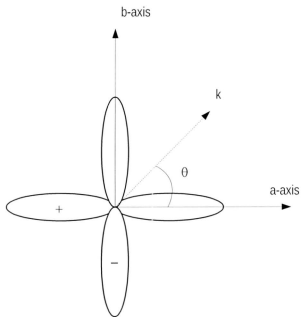
Figure 3.5: Definition of the angle θ for a $d_{x^2-y^2}$-wave superconductor. For this case, it is defined as the angle between the injection k-vector and the a-axis of the crystal [22].
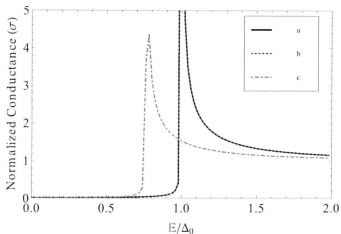
Figure 3.6: c-axis conductance spectra for: (a) $d_{x^2-y^2}$ wave with $\Delta_1 = \Delta_0$; (b) extended s wave with $\Delta_1 = 0.7\Delta_0$ and $\Delta_2 = 0.3\Delta_0$; (c) $s + id_{x^2-y^2}$ with $\Delta_1 = 0.7\Delta_0$ and $\Delta_2 = 0.3\Delta_0$.

where θ is the injection angle. Figures 3.7, 3.8 and 3.9 show the conductance spectra for these three superconductors.

In the next section we will see how these results can be extended to the case of triplet pair potentials where spin of the particles becomes important in solving the BdG equations [27].

3.2   2D system with triplet pair potential

In this Section, we analyze the tunneling conductance spectra of normal-metal/insulator/triplet superconductor junctions by extending the theory that we developed in previous sections for anisotropic singlet superconductors. In particular, we will investigate the spin dependence of the conductance spectra and the influence of the non-unitary
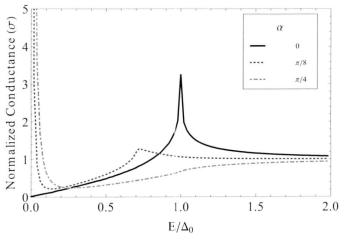
Figure 3.7: *ab*-plane conductance spectrum for a $d_{x^2-y^2}$ wave superconductor with $\Delta_1 = \Delta_0$ (a) $\alpha = 0$; (b) $\alpha = \pi/4$ and (c) $\alpha = \pi/8$.
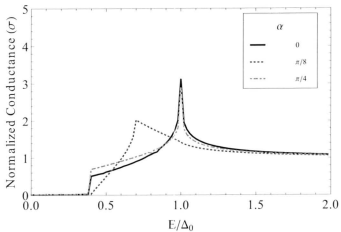
Figure 3.8: *ab*-plane conductance spectrum for an extended *s* wave superconductor with $\Delta_1 = 0.7\Delta_0$ and $\Delta_2 = 0.3\Delta_0$ (a) $\alpha = 0$; (b) $\alpha = \pi/4$ and (c) $\alpha = \pi/8$.
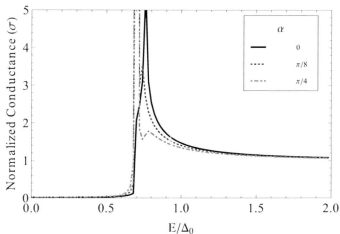
Figure 3.9: ab-plane conductance spectrum for a $s+id_{x^2-y^2}$ wave superconductor with $\Delta_1 = 0.7\Delta_0$ and $\Delta_2 = 0.3\Delta_0$ (a) $\alpha = 0$; (b) $\alpha = \pi/4$ and (c) $\alpha = \pi/8$.

states on the final results.

3.2.1 Spin dependent BdG equations

In the case of triplet superconductors, the spin structure of the pair potential should be included in the calculations. As a result, the BdG equations cannot be in general decoupled into separate equations and the spin part of the equations plays an important role in the calculations. In this case, the state of the quasi-particles are described by four-spinors in Nambu (particle-hole⊗spin) space [29]. These four-spinors

are determined by the solution of the BdG equations [25, 2, 28]

$$\begin{pmatrix} (H_0 - E)\hat{\sigma}_0 & \hat{\Delta} \\ \hat{\Delta}^\dagger & -(H_0^\dagger + E)\hat{\sigma}_0 \end{pmatrix} \begin{pmatrix} u_\uparrow(\mathbf{r}) \\ u_\downarrow(\mathbf{r}) \\ v_\uparrow(\mathbf{r}) \\ v_\downarrow(\mathbf{r}) \end{pmatrix} = 0 \qquad (3.36)$$

where $H_0 = (-\hbar^2\nabla^2/2m - E_F)\hat{\sigma}_0$ and E is the energy of the particles with

$$\hat{\sigma}_0 = \begin{pmatrix} 1 & 0 \\ 0 & 1 \end{pmatrix}. \qquad (3.37)$$

$u_\uparrow(\mathbf{r})$ corresponds to an ELQ with spin up while $u_\downarrow(\mathbf{r})$ describes the state of an ELQ with spin down. $v_\uparrow(\mathbf{r})$ and $v_\downarrow(\mathbf{r})$ corresponds to a HLQ with spin up and down, respectively.

Similar to the singlet superconductor case, an injected electron with spin up can undergo four different processes at the interface. However, this time each process can happen with two spin possibilities (up or down). Therefore, there are eight scattering processes at the interface in total whose probabilities can be found by applying the appropriate boundary conditions. Figure 3.10 illustrates these possible processes at the interface of a N/S junction.

Equation (3.36) can be written in the following form

$$Eu_s(\mathbf{r}) = -(\frac{\hbar^2}{2m}\hat{\Delta} + E_F)u_s(\mathbf{r}) + \sum_{s'}\Delta_{ss'}v_{s'}(\mathbf{r})$$
$$Ev_s(\mathbf{r}) = (\frac{\hbar^2}{2m}\hat{\Delta} + E_F)v_s(\mathbf{r}) + \sum_{s'}\Delta_{ss'}^*u_{s'}(\mathbf{r}). \qquad (3.38)$$

In these equations, spin index s can take two values $\uparrow$ and $\downarrow$, $\mathbf{k}$ represents the relative motion of the Cooper pairs fixed on the Fermi surface ($|\mathbf{k}| = k_F$) and $\mathbf{r}$ describes the center of mass coordinates of the Cooper pair. We also assume that the Fermi wave vector is the same on both sides of the junction [30].

3.2.2 Spin dependent normalized conductance

Because of translational symmetry at the interface of the junction, only z-component of the present wave vector in the problem contribute to the final result. Hence, following the BTK model, the solution of Equation (3.36) can be written as the linear combination of possible scattering processes. Considering an injected electron with spin up, for $z < 0$ the wave function of the system is given by [2, 30, 31]

$$\psi_N = (1 + b_{\uparrow\uparrow}) \begin{pmatrix} 1 \\ 0 \\ 0 \\ 0 \end{pmatrix} e^{ik_z^{N+}z} + b_{\uparrow\downarrow} \begin{pmatrix} 0 \\ 1 \\ 0 \\ 0 \end{pmatrix} e^{-ik_z^{N+}z} + a_{\uparrow\uparrow} \begin{pmatrix} 0 \\ 0 \\ 1 \\ 0 \end{pmatrix} e^{ik_z^{N-}z} + a_{\uparrow\downarrow} \begin{pmatrix} 0 \\ 0 \\ 0 \\ 1 \end{pmatrix} e^{ik_z^{N-}z}.$$
(3.39)

For $z \geq 0$, the solution can be written as

$$\psi_S = \left[c_{\uparrow 1} \begin{pmatrix} U_{11} \\ U_{21} \\ U_{31} \\ U_{41} \end{pmatrix} + c_{\uparrow 2} \begin{pmatrix} U_{12} \\ U_{22} \\ U_{32} \\ U_{42} \end{pmatrix} \right] e^{-ik_z^{S+}z} + \left[d_{\uparrow 1} \begin{pmatrix} U_{13} \\ U_{23} \\ U_{33} \\ U_{43} \end{pmatrix} + d_{\uparrow 2} \begin{pmatrix} U_{14} \\ U_{24} \\ U_{34} \\ U_{44} \end{pmatrix} \right] e^{ik_z^{S-}z}.$$
(3.40)

The coefficients used in these equations are:

a, the coefficients of Andreev reflection;
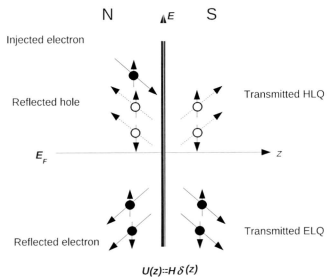
Figure 3.10: Schematic illustration of the reflection and the transmission process of an injected electron with spin up at the interface of a normal-metal/triplet-superconductor junction.

b, the reflection coefficients of normal reflection;

c, the probability amplitude of transmission as an ELQ; and

d, the probability amplitude of transmission as a HLQ.

Finally, U_{ij} are the components of the Bogoliubov (unitary) transformation matrix [2] (see Appendix A).

For example, $b_{\uparrow\uparrow}$ is the probability amplitude of normal reflection with spin up, when the injected particle is a spin up electron, while $a_{\uparrow\downarrow}$ is Andreev reflection of a spin down hole.

In the weak coupling limit, the amplitude of all the wave vectors are fixed to the Fermi surface such that

$$k_z^{N+} = k_z^{N-} = k_z^{S+} = k_z^{S-} \approx k_F \cos\theta \qquad (3.41)$$

where θ is measured with respect to normal to the interface (z-axis). The rest of the unknowns can be found using the appropriate boundary conditions

$$\psi_S(z)\mid_{z=0+} = \psi_N(z)\mid_{z=0-} \qquad (3.42)$$

$$\frac{d}{dz}\psi_S(z)\mid_{z=0+} - \frac{d}{dz}\psi_N(z)\mid_{z=0-} = \frac{2mH}{\hbar^2}\psi_N(z)\mid_{z=0-} . \qquad (3.43)$$

The general form of these coefficients are given in Appendix B.

Finally, by finding these coefficients for both spin up and spin down injection we can calculate the normalized conductance $\sigma(E)$ of the junction which is given by [30, 32]

$$\sigma(E) = \frac{\int_{-\pi/2}^{\pi/2} (\sigma_{S\uparrow} + \sigma_{S\downarrow}) \cos\theta \; d\theta}{\int_{-\pi/2}^{\pi/2} 2 \; \sigma_N \; \cos\theta \; d\theta} \tag{3.44}$$

where $\sigma_{S\uparrow}$ and $\sigma_{S\downarrow}$ are the conductance of the junction for spin up and spin down injection at a given angle θ, respectively. These two functions are defined as

$$\begin{aligned}
\sigma_{S\uparrow} &= 1 + \mid a_{\uparrow\uparrow} \mid^2 + \mid a_{\uparrow\downarrow} \mid^2 - \mid b_{\uparrow\uparrow} \mid^2 - \mid b_{\uparrow\downarrow} \mid^2 \\
\sigma_{S\downarrow} &= 1 + \mid a_{\downarrow\uparrow} \mid^2 + \mid a_{\downarrow\downarrow} \mid^2 - \mid b_{\downarrow\uparrow} \mid^2 - \mid b_{\downarrow\downarrow} \mid^2 .
\end{aligned} \tag{3.45}$$

The normal conductance of the junction σ_N is given by

$$\begin{aligned}
\sigma_N &= \frac{\cos^2\theta}{\cos^2\theta + Z^2} \\
Z &= \frac{mH}{\hbar^2 k_F}.
\end{aligned} \tag{3.46}$$

In the next Section we will review the conductance spectra of some N/S junctions with triplet pair potential superconductivity.

3.2.3 Conductance spectra of 2D normal-metal/triplet superconductor junctions

In this Section we calculate the conductance spectrum of a junction with a spin-triplet superconductor for both unitary and non-unitary gap functions. In general, for triplet superconducting states the gap function is parametrized by a vector function $\mathbf{d}(\mathbf{k})$ (see Appendix A)

$$\Delta(\mathbf{k}) = i\sigma_2(\mathbf{d}(\mathbf{k}) \cdot \sigma) \tag{3.47}$$

where $\mathbf{d}(\mathbf{k})$ is an odd function of $\mathbf{k}$ [2].

In 2D, the most symmetric unitary triplet state is given by

$$\mathbf{d}(\mathbf{k}) \propto \hat{\mathbf{x}}k_x + \hat{\mathbf{y}}k_y. \tag{3.48}$$

Also, a simple example of non-unitary state is written as

$$\mathbf{d}(\mathbf{k}) \propto (\hat{\mathbf{x}} + i\hat{\mathbf{y}})(k_x - ik_y). \tag{3.49}$$

From these vectors, we can form the appropriate gap function which is used in turn to calculate the normalized conductance.

3.2.3.1   Unitary example

Using (3.48), the gap function is

$$\Delta(\mathbf{k}) = \Delta_0 \begin{pmatrix} -k_x + ik_y & 0 \\ 0 & k_x + ik_y \end{pmatrix}. \tag{3.50}$$

In cylindrical coordinates, this matrix is rewritten as,

$$\Delta(\mathbf{k}) = \Delta_0' \begin{pmatrix} -\cos\theta + i\sin\theta & 0 \\ 0 & \cos\theta + i\sin\theta \end{pmatrix}. \tag{3.51}$$

This matrix is used to find the normalized conductance spectrum of the junction, shown in Figure 3.11 for various Z values.
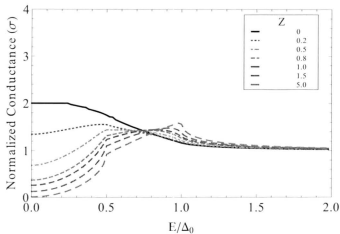
Figure 3.11: Normalized conductance of normal-metal/insulator/unitary-triplet superconductor junction for various Z values.

3.2.3.2 Non-unitary example

Using (3.49), the gap function is

$$\Delta(\mathbf{k}) = \Delta_0 \begin{pmatrix} -k_x + ik_y & 0 \\ 0 & 0 \end{pmatrix} \tag{3.52}$$

or

$$\Delta(\mathbf{k}) = \Delta'_0 \begin{pmatrix} -\cos\theta + i\sin\theta & 0 \\ 0 & 0 \end{pmatrix}. \tag{3.53}$$

This matrix results in a conductance spectrum as is shown in Figure 3.12.
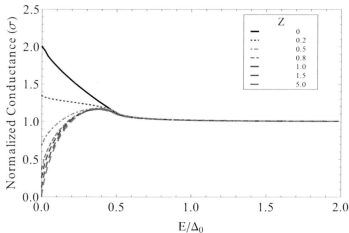
Figure 3.12: Normalized conductance of normal-metal/insulator/nonunitary-triplet superconductor junction for various Z values.

3.3 3D system

The results of the two dimensional calculations are only applicable to junctions which are made of superconductors whose pairing potentials are invariant in the third direction. For superconductors that are three dimensional, we have to extend our model to three dimensions. However, since the transverse components of the momentum vector are conserved, the different scattering processes always take place in the plane of these components [22, 30, 32]. Hence, the BdG equations are confined to this plane and the problem can be reduced to two dimensions. However, the pair potential depends on all three components of the $\mathbf{k}$ vector (we assume Δ has no spatial variation),

$$\Delta(\mathbf{k}, \mathbf{r}) = \Delta(\mathbf{k})\Theta(z) \tag{3.54}$$

(where the junction interface is perpendicular to z-axis). Therefore, after finding the corresponding conductance coefficients, the normalized conductance integration is carried over a three dimensional solid angle, covering the half of the Fermi surface with $k_z > 0$. Using spherical coordinates, the conductance is given by following formula

$$\sigma(E) = \frac{\int \left(\sigma_{S\uparrow}(\theta, \phi, E) + \sigma_{S\downarrow}(\theta, \phi, E)\right) d\Omega}{\int 2 \sigma_N d\Omega} \tag{3.55}$$

where θ and ϕ are polar and azimuthal coordinates, respectively.

The superconductor that we are studying in this work ($PrOs_4Sb_{12}$) is cubic. Therefore, analyzing the conductance spectrum of normal-metal/$PrOs_4Sb_{12}$ junctions requires a 3D treatment. In the next Chapter we will present three dimensional calculations of tunneling conductance of such a junction using various candidates as the pair potential of $PrOs_4Sb_{12}$.

Chapter 4

Conductance spectrum for Normal-Metal/Insulator/PrOs$_4$Sb$_{12}$ Junctions

As already mentioned in Chapter 1, the superconducting gap topology of PrOs$_4$Sb$_{12}$ has been the subject of variety of experimental studies. However, none of these experiments has confirmed the actual symmetry of the superconducting phase in this material [33, 34, 35, 36, 37, 38]. PCARS, known as a local probe of electronic structure, provides us further information about the symmetry of the superconducting gap. This information can be used along with results of other experiments to find a more accurate picture about the structure of the gap function of PrOs$_4$Sb$_{12}$.

By using the formalism developed in previous chapters, in this chapter we calculate the conductance spectrum of a Normal-Metal/Insulator/PrOs$_4$Sb$_{12}$ junction. The cubic symmetry of PrOs$_4$Sb$_{12}$ crystal structure forces us to employ a 3D analysis of the spectrum. The conductance can be calculated for various superconducting gap

Figure 4.1: Schematic illustration of normal-metal/insulator/PrOs$_4$Sb$_{12}$ junction. The interface is located at $z = 0$ and is perpendicular to z-axis.

symmetries. One of these possible symmetries is expected to be the symmetry of the superconducting phase in PrOs$_4$Sb$_{12}$.

In general, applying the phenomenological Landau theory to crystal symmetry group of PrOs$_4$Sb$_{12}$ provides us with all the possible symmetry groups of superconducting gap [39, 3]. These symmetry candidates can be divided into two groups: singlet and triplet pair potentials.

In the following sections, we will explain the model which our conductance calculation is based on it. Then we will report the result for each group (singlet and triplet) separately.

4.1 Normal-Metal/Insulator/PrOs$_4$Sb$_{12}$ Junction

4.1.1 Set-up

Throughout this chapter we consider a junction as it is shown in Figure 4.1. According to this picture, electrons are injected into the superconductor with wave vector (k_x, k_y, k_z) such that $k_z > 0$. The interface is located at $z = 0$ and it is described by $H\delta(z)$. All the scattering processes at the interface take place in a two dimensional plane which is defined by a fixed angle ϕ in the spherical coordinate system. In this system, the wave vector of the incident electrons are written as

$$\mathbf{k} = k_F(\sin\theta\cos\phi, \sin\theta\sin\phi, \cos\theta) \tag{4.1}$$

where we assumed that the amplitude of this vector is fixed to the Fermi surface (weak coupling limit approximation). $k_z > 0$ implies the following condition on the range of azimuthal and polar angles

$$\begin{aligned} 0 &< \phi < 2\pi \\ 0 &< \theta < \pi/2 \end{aligned} \tag{4.2}$$

In addition, the possible scattering processes are shown in Figure 4.2. The conductance coefficients are generally a function of θ, ϕ and E for this configuration. Since the amplitude of the Fermi energy is the same on both sides of the junction ($E_{FN} = E_{FS}$), all the particles in the problem make the same angle θ with the normal to the interface (z-axis)

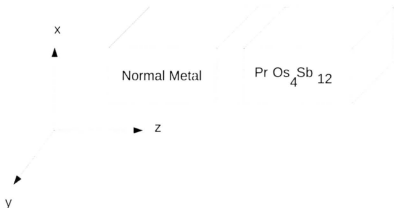$$k_z^{N+} = k_z^{N-} = k_z^{S+} = k_z^{S-} = k_F\cos\theta \tag{4.3}$$
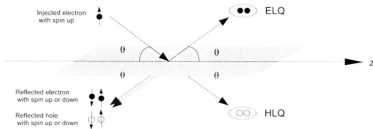
Figure 4.2: Schematic illustration of normal-metal/insulator/PrOs$_4$Sb$_{12}$ junction. The interface is located at $z = 0$ and is perpendicular to the z-axis.

4.1.2   Conductance

Once the conductance coefficients are found, the normalized conductance is calculated by integration over the hemisphere in k-space defined by

$$k_z > 0$$
$$0 < \phi < 2\pi$$
$$0 < \theta < \pi/2.$$

(4.4)

Therefore, using the spherical solid angle, the normalized conductance is written as

$$\sigma(E) = \frac{\int_0^{2\pi} \int_0^{\pi/2} \left(\sigma_{S\uparrow}(E, \theta, \phi) + \sigma_{S\downarrow}(E, \theta, \phi) \right) \, \sin\theta \, d\theta d\phi}{\int_0^{2\pi} \int_0^{\pi/2} 2 \, \sigma_N \, \sin\theta \, d\theta d\phi}$$

(4.5)

where the normal conductance σ_N for this particular configuration is given by

$$\sigma_N = \frac{\cos^2\theta}{\cos^2\theta + Z^2}$$

(4.6)

and so the denominator of Equation (4.5) is $4\pi \int_0^{\pi/2} \sigma_N \, \sin\theta \, d\theta$.

In general, σ_N can be obtained through angle-resolved conductance formula, once Δ vanishes,

$$\sigma_N = \lim_{\Delta \to 0} \sigma_S \qquad (4.7)$$

It may be noted that, although $\sigma_{S\uparrow}$ and $\sigma_{S\downarrow}$ are generally two different functions, they become equal for singlet pair potentials and those triplet states that are unitary.

4.2   Singlet states

For a singlet pair potential which is antisymmetric under exchange, Δ is an even function of $\mathbf{k}$, since the whole state is antisymmetric. Therefore the antisymmetric matrix $\Delta(\mathbf{k})$ is parametrised by a single even function $\psi(\mathbf{k})$

$$\Delta(\mathbf{k}) = i\sigma_y \psi(\mathbf{k}) = \begin{pmatrix} 0 & \psi(\mathbf{k}) \\ -\psi(\mathbf{k}) & 0 \end{pmatrix} \qquad (4.8)$$

Tetrahedral point group T_h (the point group of $PrOs_4Sb_12$) has 1D, 2D and 3D order parameters in each of the singlet and triplet channels [3]. The 1D order parameter in the singlet channel is nothing more than ordinary s-wave symmetry which has no nodes at all.

The 2D order parameter includes two phases that are accessible from the normal state. The first phase has $T(D_2)$ symmetry. This phase includes eight point nodes and three equivalent domains.

The second phase of 2D order parameter has $D_2 \times K$ symmetry group, a subgroup of T_h. Since the s-wave superconductivity may appear as a secondary order parameter in this phase and remove the nodes in the gap function, we do not consider this case

in our calculations.

There are four phases for 3D order parameter accessible from the normal state. The first phase has symmetry $T(D_2) \times K$ and contains three domains. This phase has line nodes. The second phase has $C_3 \times K$ symmetry. This phase includes s-wave as its secondary order parameter and hence of no particular interest. The third phase is probably not an acceptable candidate for superconductivity because of its three-fold symmetry. However, we consider this case in present work. It has $C_3(E)$ symmetry.

Finally, we consider the fourth phase with symmetry $D_2(E)$ which also has line nodes.

In the following section we will present the conductance spectrum calculation for each of aforementioned cases.

4.2.1 Case one: $T(D_2)$

This case is the first phase of 2D order parameter with components $(1, 0)$. The gap function is described by

$$\begin{aligned}
\psi(k) &\sim \epsilon k_x^2 + \epsilon^2 k_y^2 + k_z^2 \\
&\sim \Delta_0 \left(\cos^2 \theta - \frac{\sin^2 \theta}{2} + i \frac{\sqrt{3}}{2} \sin^2 \theta \cos 2\phi \right)
\end{aligned} \tag{4.9}$$

This gap function is complex. By using the above gap function, we can calculate the conductance which is shown in Figure 4.3.
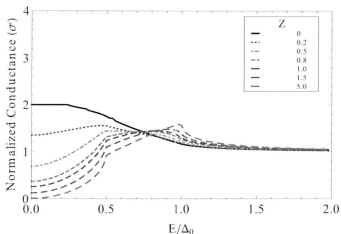
Figure 4.3: Normalized conductance of normal-metal/insulator/PrOs$_4$Sb$_{12}$ junction with singlet-$T(D_2)$,$(1,0)$ state for various Z values.

4.2.2 Case two: $D_2(C_2) \times K$

This case has has three domains. The gap function for the first domain is given by

$$\psi(k) \sim k_y k_z$$
$$\sim \frac{\Delta_0}{2} \sin 2\theta \sin \phi. \tag{4.10}$$

This gap function results in a conductance spectrum shown in Figure 4.4. The second domain has $\psi(k) \sim k_x k_z$, which results in the same spectrum as the first. The third domain is defined by

$$\psi(k) \sim k_x k_y$$
$$\sim \frac{\Delta_0}{2} \sin^2 \theta \sin 2\phi \tag{4.11}$$

and Figure 4.5 shows the corresponding spectrum. As it can be seen from this figure,

Figure 4.4: Normalized conductance of normal-metal/insulator/PrOs$_4$Sb$_{12}$ junction with singlet-$D_2(C_2) \times K$ state in first domain for various Z values.

the conductance at some points is different from the first domain's spectrum. In particular, there is no zero bias conductance peak in the second spectrum.

4.2.3 Case three: $C_3(E)$

The gap function is defined by

$$
\begin{aligned}
\psi(k) &\sim \epsilon k_y k_x + \epsilon^2 k_z k_z + k_y k_x \\
&\sim \frac{\Delta_0}{4}(2\sin^2\theta\sin 2\phi - \sin 2\theta\sin\phi - \sin 2\theta\cos\phi \\
&+ i\sqrt{3}\sin 2\theta(\sin\phi - \cos\phi))
\end{aligned}
\tag{4.12}
$$

Figure 4.6 illustrates the conductance spectrum for this case.
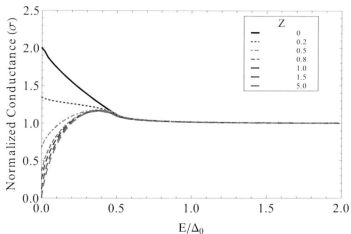
Figure 4.5: Normalized conductance of normal-metal/insulator/PrOs$_4$Sb$_{12}$ junction with singlet-$D_2(C_2) \times K$ state in third domain for various Z values.
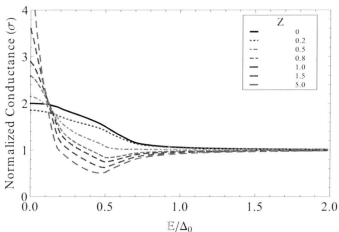
Figure 4.6: Normalized conductance of normal-metal/insulator/PrOs$_4$Sb$_{12}$ junction with singlet-$C_3(E)$ state for various Z values.
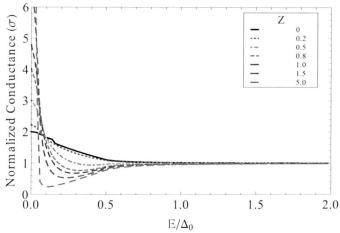
Figure 4.7: Normalized conductance of normal-metal/insulator/PrOs$_4$Sb$_{12}$ junction with singlet-$D_2(E)$ state in first domain for various Z values. The ratio of Δ_0/Δ_1 is set to 10.

4.2.4 Case four: $D_2(E)$

This case has three domains the first of which is described by

$$
\begin{aligned}
\psi(k) &= |\eta_1|k_x k_z + i|\eta_2|k_x k_y \\
&\sim \frac{\Delta_0}{2}\sin 2\theta \cos\phi + i\frac{\Delta_1}{2}\sin^2\theta \sin 2\phi.
\end{aligned}
\tag{4.13}
$$

The corresponding conductance spectrum is shown is Figure 4.7.

The second domain is introduced by

$$
\begin{aligned}
\psi(k) &= |\eta_1|k_y k_z + i|\eta_2|k_x k_y \\
&\sim \frac{\Delta_0}{2}\sin 2\theta \sin\phi + i\frac{\Delta_1}{2}\sin 2\theta \cos\phi
\end{aligned}
\tag{4.14}
$$

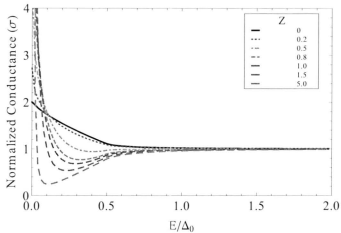and the third domain is $\psi(k) = |\eta_1|k_x k_z + i|\eta_2|k_y k_z$.
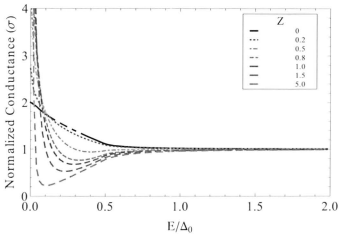
Figure 4.8: Normalized conductance of normal-metal/insulator/PrOs$_4$Sb$_{12}$ junction with singlet-$D_2(E)$ state in second domain for various Z values. The ratio of Δ_0/Δ_1 is set to 10.

For this symmetry the shape of the conductance spectrum for the first and the second domains is almost the same.

4.3 Triplet states

Triplet pair potential is an odd function of $\mathbf{k}$. In general, the $\Delta(\mathbf{k})$ matrix is given by

$$\Delta(\mathbf{k}) = i(\mathbf{d}(\mathbf{k}) \cdot \hat{\sigma})\sigma_y = \begin{pmatrix} -d_x(\mathbf{k}) + id_y(\mathbf{k}) & d_z(\mathbf{k}) \\ d_z(\mathbf{k}) & d_x(\mathbf{k}) + id_y(\mathbf{k}) \end{pmatrix} \tag{4.15}$$

where $\mathbf{d}(\mathbf{k})$ is an odd vectorial function (see Appendix A). According to this definition this matrix is always symmetric.

Similar to the singlet case, the triplet case can be divided to 1D, 2D and 3D order parameter. These order parameters which are already introduced has the same properties as the singlet case (same symmetry, domains and etc.). However, there are some differences between singlet and triplet order parameters. In particular, the first phase of 2D order parameter and the third and fourth phase of 3D order parameter are non-unitary states. In general, for these non-unitary states, we have to calculate the conductance for both spin up and spin down injection since these conductances are not the same any more. As already mentioned, the normalized conductance is obtained by adding these two functions together. The conductance spectrum of the triplet states can be found in the following which are divided into unitary and non-unitary cases.

4.3.1 Unitary pair potentials

4.3.1.1 Case one: $T \times K$

This is a 1D order parameter. The gap function is defined by a simple $\mathbf{d}$ vector

$$\mathbf{d}(\mathbf{k}) \sim (k_x, k_y, k_z) \tag{4.16}$$

The corresponding gap function is given by

$$\Delta(\mathbf{k}) = \begin{pmatrix} -k_x + ik_y & k_z \\ k_z & k_x + ik_y \end{pmatrix}. \tag{4.17}$$

This matrix can be written in a more useful way since we assume all the wave vectors are fixed to k_F

$$\Delta(\mathbf{k}) = \Delta_0 \begin{pmatrix} -\sin\theta e^{-i\phi} & \cos\theta \\ \cos\theta & \sin\theta e^{i\phi} \end{pmatrix}. \tag{4.18}$$

Figure 4.9: Normalized conductance of normal-metal/insulator/PrOs$_4$Sb$_{12}$ junction with unitary triplet-T state for various Z values [40].

The corresponding conductance spectrum is shown in figure 4.9.

4.3.1.2 Case two: $D_2(C_2) \times K$

This is a 3D order parameter which has three domains. The first domain is defined by $\mathbf{d}(\mathbf{k}) \sim (0, bk_z, ak_y)$ and the gap function is given by

$$\Delta(\mathbf{k}) = \begin{pmatrix} i\Delta_0 \cos\theta & \Delta_1 \sin\theta \sin\phi \\ \Delta_1 \sin\theta \sin\phi & i\Delta_0 \cos\theta \end{pmatrix} \tag{4.19}$$

where Δ_0 and Δ_1 are two arbitrary parameters.

The second domain is characterized by $\mathbf{d}(\mathbf{k}) \sim (bk_y, ak_x, 0)$. The following gap func-

Figure 4.10: Normalized conductance of normal-metal/insulator/PrOs$_4$Sb$_{12}$ junction with unitary triplet-$D_2(C_2)$ state in first domain for various Z values. From top to bottom the ratio of Δ_0/Δ_1 is set to 10, 1 and 0.1 respectively [40].
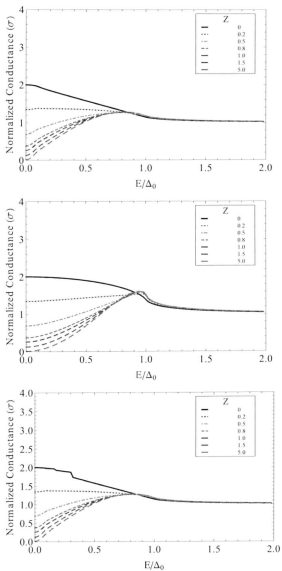
Figure 4.11: Normalized conductance of normal-metal/insulator/PrOs$_4$Sb$_{12}$ junction with unitary triplet-$D_2(C_2)$ state in second domain for various Z values. From top to bottom the ratio of Δ_0/Δ_1 is set to 10, 1 and 0.1 respectively [40].

tion can be built using this vector

$$\Delta(\mathbf{k}) = \begin{pmatrix} -\Delta_0 \sin\theta \sin\phi + i\Delta_1 \sin\theta \cos\phi & 0 \\ 0 & \Delta_0 \sin\theta \sin\phi + i\Delta_1 \sin\theta \cos\phi \end{pmatrix} \quad (4.20)$$

Figures 4.10 and 4.11 illustrates conductance spectrum for these two domains. The third domain is $\mathbf{d}(\mathbf{k}) \sim (ak_z, 0, bk_y)$ and yields results equivalent to the first domain.

4.3.2 Non-unitary pair potentials

4.3.2.1 Case one: $T(D_2)$

This 2D order parameter is shown by $\mathbf{d}(\mathbf{k}) \sim (\epsilon k_x, \epsilon^2 k_y, k_z)$ which results in

$$\Delta(\mathbf{k}) = \Delta_0 \begin{pmatrix} -\epsilon \sin\theta \cos\phi + i\epsilon^2 \sin\theta \sin\phi & \cos\theta \\ \cos\theta & \epsilon \sin\theta \cos\phi + i\epsilon^2 \sin\theta \sin\phi \end{pmatrix} \quad (4.21)$$

where $\epsilon = \exp(+i2\pi/3)$. In addition, the $\mathbf{q}$ vector (which characterizes the non-unitary states, see Appendix A) for this case can be written as

$$\mathbf{q}(\mathbf{k}) = \sqrt{3}(k_y k_z, k_z k_x, k_x k_y) \quad (4.22)$$

The conductance spectrum for this non-unitary case is seen in Figure 4.12.

4.3.2.2 Case two: $C_3(E)$

This 3D non-unitary order parameter has $(\epsilon, \epsilon^2, 1)$ components. The $\mathbf{d}$ vector for this case is more complicated and has three non zero components

$$\mathbf{d}(\mathbf{k}) = (\epsilon^2 ak_z + bk_y, \epsilon bk_z + ak_x, \epsilon ak_y + \epsilon^2 bk_x) \quad (4.23)$$
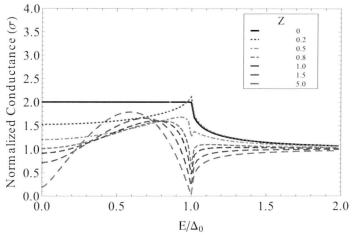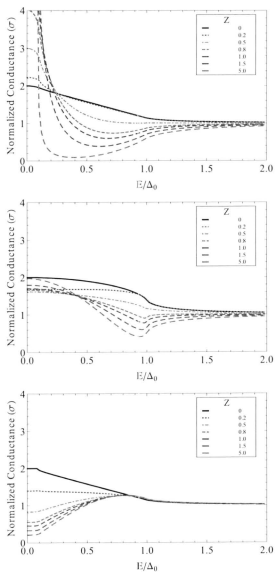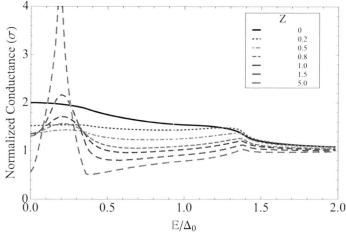
Figure 4.12: Normalized conductance of normal-metal/insulator/PrOs$_4$Sb$_{12}$ junction with non-unitary triplet-$T(D_2)$ state for various Z values [40].

This vector results in the following $\mathbf{q}$ vector

$$\mathbf{q}(\mathbf{k}) = \sqrt{3}(b^2 k_z k_x + a^2 k_y k_z - abk_x^2, a^2 k_y k_z + b^2 k_z k_y - abk_y^2, a^2 k_x k_z + b^2 k_y k_z - abk_z^2)$$

(4.24)

The conductance spectrum for this case is represented in Figure 4.13.

4.4 Summary

The conductance spectra calculated in previous sections show important features in both singlet and triplet channels which are helpful for finding superconducting state in PrOs$_4$Sb$_{12}$. ZBCP is one of the most important features which appears in many of these spectra. This feature is known as a main characteristic of gap functions with nodes. Hence, if experimental PCARS results show a conductance spectrum with ZBCP for PrOs$_4$Sb$_{12}$, then one could expect that superconductivity in PrOs$_4$Sb$_{12}$ is
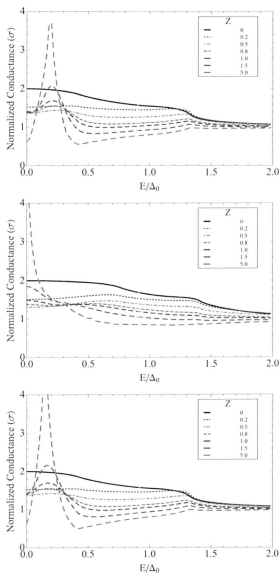
Figure 4.13: Normalized conductance of normal-metal/insulator/PrOs$_4$Sb$_{12}$ junction with non-unitary triplet-$C_3(E)$ state for various Z values. From top to bottom the ratio of Δ_0/Δ_1 is set to 10, 1 and 0.1 respectively [40].

unconventional [41].

In general, these results provide a powerful way of studying superconductivity in $PrOs_4Sb_{12}$ if they are combined with experimental results.

Chapter 5

Conclusion

The overall objective of this work was to investigate the symmetry of the superconducting state in $PrOs_4Sb_{12}$ by means of PCARS. The symmetry of the crystal in its normal state in $PrOs_4Sb_{12}$ is described by T_h point group. This point group is the starting point of studying the symmetry of the superconducting order parameter based on phenomenological Landau theory. In fact, order parameters are classified according to representations of the point group of the crystal. In $PrOs_4Sb_{12}$ case, these order parameters can be categorized into one dimensional, two dimensional and three dimensional irreducible representations (one of each) where each representation can be further divided into spin-singlet (even) and spin-triplet (odd) channels. Based on experimental data, some of these states are more likely to be responsible for superconductivity in $PrOs_4Sb_{12}$.

PCARS method is based on the information that can be extracted from the normalized conductance spectrum of a normal-metal/superconductor junction. The starting point of conductance calculations is to understand the scattering processes an injected particle may undergo at the interface of the junction. This can be performed

by using the BdG equations together with BTK model. The conductance problem for $PrOs_4Sb_{12}$ is three dimensional since it has cubic symmetry. In order to find the conductance coefficients we employed a combination of analytical and computational methods.

The calculated conductance spectrum for each order parameter of $PrOs_4Sb_{12}$ shows many interesting features including peaks at different energy points. These features can be interpreted by developing appropriate theories about tunneling phenomena which occur at the interface of the junction. Besides the theoretical aspects of these results, the main purpose of this work was to provide a complete catalog of conductance spectrum for various superconductivity candidates in $PrOs_4Sb_{12}$. This catalog can be used along with any experimental work in order to investigate the actual superconducting phase of $PrOs_4Sb_{12}$.

In general, experimental results show some additional features which cannot be observed in this theoretical work. However, these features can be a consequence of experimental conditions which may include sample preparation, the quality of the contact and etc. Despite these minor differences, comparing the overall shape of the experimental and theoretical spectrum is a reliable way of analyzing superconducting state in $PrOs_4Sb_{12}$. In particular, outstanding features such as conductance peaks and singularities are believed to be independent of experimental inaccuracy.

Further information about the superconducting gap could be obtained by using spin polarized current in the junction. This is possible by using a ferromagnet/superconductor instead of normal-metal/superconductor junction. In this case, the properties of Andreev reflection are significantly modified. In this way, one can even find more

information about the structure of the superconducting pairs in a superconductor.

Using a multi-band order parameter is the other direction in which this work can be generalized. Although it has not been proved yet, variety of experimental results can be interpreted by considering a multi-band superconductivity for $PrOs_4Sb_{12}$. This scenario may also be the source of experimentally-observed features of conductance spectrum that were not found in any of the calculations of this thesis.

Although PCARS cannot point conclusively at a particular order parameter, it can certainly rule out some possibilities. These are the 1D order parameter in both singlet and triplet channels. In particular, the theoretical PCARS calculations are consistent with some experimental results obtained recently [42]. The main characteristics of these results are appearance of ZBCP and non-zero spectral weight. These features can be observed in the conductance spectrum of many of the 3D triplet symmetries investigated in Chapter 3. Therefore, we can conclude that superconductivity in $PrOs_4Sb_{12}$ is unconventional, and most likely belongs to the 3D representation in the triplet channel. However, more experimental efforts are requires in order to specify the exact symmetry of superconducting phase in $PrOs_4Sb_{12}$.

Appendix A

Generalized theory of superconductivity

According to the BCS[1] theory [1], the appearance of superconductivity in materials is associated with formation of a pair of conduction electrons. In fact, in the presence of an attractive potential, the Fermi sea of conduction electrons becomes unstable. The new stable ground state is a quantum condensed state consisting of so-called Cooper pairs. In general, the attractive potential between the electrons originates from various mechanisms. In conventional superconductors, the electron-phonon interaction is the source of this potential.

Considering a pairing potential in momentum space, the effective Hamiltonian of the paired particles can be written as

$$H = \sum_{\mathbf{k},s} \varepsilon(\mathbf{k}) a^\dagger_{\mathbf{k}s} a_{\mathbf{k}s} + \frac{1}{2} \sum_{\mathbf{k},\mathbf{k}',s_1,s_2,s_3,s_4} V_{s_1 s_2 s_3 s_4}(\mathbf{k},\mathbf{k}') a^\dagger_{-\mathbf{k}s_1} a^\dagger_{\mathbf{k}s_2} a_{\mathbf{k}'s_3} a_{-\mathbf{k}'s_4}. \qquad (A.1)$$

In this equation, $\varepsilon(\mathbf{k})$ represents the band energy which is measured relative to the

---

[1]Bardeen, Cooper and Schrieffer

chemical potential μ and $V_{s_1 s_2 s_3 s_4}$ is defined as

$$\langle -\mathbf{k}, s_1; \mathbf{k}, s_2 | \hat{V} | -\mathbf{k}', s_4; \mathbf{k}', s_3 \rangle. \tag{A.2}$$

In fact, $V_{s_1 s_2 s_3 s_4}$ is the matrix element of a general effective attractive interaction between two electrons.

By defining the following mean fields, we can treat the Hamiltonian in Equation (A.1) as a many body Hamiltonian,

$$
\begin{aligned}
\Delta_{ss'}(\mathbf{k}) &= -\sum_{\mathbf{k}', s_3, s_4} V_{s'ss_3s_4}(\mathbf{k}, \mathbf{k}') \langle a_{\mathbf{k}'s_3} a_{-\mathbf{k}'s_4} \rangle \\
\Delta^*_{ss'}(-\mathbf{k}) &= -\sum_{\mathbf{k}', s_1, s_2} V_{s_1 s_2 s' s}(\mathbf{k}', \mathbf{k}) \langle a^\dagger_{-\mathbf{k}'s_1} a^\dagger_{\mathbf{k}'s_2} \rangle
\end{aligned}
\tag{A.3}
$$

where the brackets show the expectation value. Assuming small mean field fluctuations we can approximate the effective Hamiltonian by [2]

$$\tilde{H} = \sum_{\mathbf{k},s} \varepsilon(\mathbf{k}) a^\dagger_{\mathbf{k}s} a_{\mathbf{k}s} + \frac{1}{2} \sum_{\mathbf{k}, s_1, s_2} \left[\Delta_{s_1 s_2}(\mathbf{k}) a^\dagger_{\mathbf{k}s_1} a^\dagger_{-\mathbf{k}s_2} - \Delta^*_{s_1 s_2}(-\mathbf{k}) a_{-\mathbf{k}s_1} a_{\mathbf{k}s_2} \right]. \tag{A.4}$$

This new Hamiltonian is a single particle operator which can be diagonalized by a (unitary) Bogoliubov (or canonical) transformation

$$a_{\mathbf{k}s} = \sum_{s'} \left(u_{\mathbf{k}ss'} \alpha_{\mathbf{k}s'} + v_{\mathbf{k}ss'} \alpha^\dagger_{-\mathbf{k}s'} \right). \tag{A.5}$$

Here $\alpha^\dagger_a$ and α_b are the eigenoperators of the single particle Hamiltonian which satisfy

the following relations

$$\partial_t \alpha_b = i[\tilde{H}, \alpha_b] = -E_b \alpha_b$$
$$\partial_t \alpha_a^\dagger = i[\tilde{H}, \alpha_a^\dagger] = E_a \alpha_a^\dagger.$$

$$(A.6)$$

The transformation equation can be written in a more compact way by introducing a four-component notation

$$\mathbf{a_k} = (a_{\mathbf{k}\uparrow}, a_{\mathbf{k}\downarrow}, a_{-\mathbf{k}\uparrow}^\dagger, a_{-\mathbf{k}\downarrow}^\dagger)$$
$$\alpha_{\mathbf{k}} = (\alpha_{\mathbf{k}\uparrow}, \alpha_{\mathbf{k}\downarrow}, \alpha_{-\mathbf{k}\uparrow}^\dagger, \alpha_{-\mathbf{k}\downarrow}^\dagger)$$

$$(A.7)$$

then

$$\mathbf{a_k} = U_k \alpha_{\mathbf{k}}.$$

$$(A.8)$$

Here U_k is the unitary transformation matrix which is defined in terms of the 2×2 matrices of Equation (A.5)

$$U_k = \begin{bmatrix} \hat{u}_k & \hat{v}_k \\ \hat{v}_{-k}^* & \hat{u}_{-k}^* \end{bmatrix}$$

$$(A.9)$$

where $U_k U_k^\dagger = 1$.

Following this notation and by defining the eigenvalues matrix

$$\hat{E}_{\mathbf{k}} = \begin{bmatrix} E_{\mathbf{k}+} & 0 & 0 & 0 \\ 0 & E_{\mathbf{k}-} & 0 & 0 \\ 0 & 0 & -E_{-\mathbf{k}+} & 0 \\ 0 & 0 & 0 & -E_{-\mathbf{k}-} \end{bmatrix}$$

$$(A.10)$$

the diagonalization of $\tilde{H}$ is given by

$$\hat{E}_{\mathbf{k}} = U_{\mathbf{k}}^{\dagger} \hat{\mathcal{E}}_k U_{\mathbf{k}} \tag{A.11}$$

where $\hat{\mathcal{E}}_k$ is the 4×4 representation of $\tilde{H}$.

$$\hat{\mathcal{E}}_k = \begin{bmatrix} \epsilon(\mathbf{k})\hat{\sigma}_0 & \hat{\Delta}(\mathbf{k}) \\ -\hat{\Delta}^*(-\mathbf{k}) & -\epsilon(\mathbf{k})\hat{\sigma}_0 \end{bmatrix} \tag{A.12}$$

where $\hat{\Delta}(\mathbf{k})$ is the 2×2 gap function matrix, defined below.

In general, symmetry of $\hat{\Delta}(\mathbf{k})$ in k-space is the same as the symmetry of pairing wave function. Therefore, since the total wave function of fermions is antisymmetric, we can write for $\hat{\Delta}(\mathbf{k})$

$$\hat{\Delta}(\mathbf{k}) = -\hat{\Delta}^T(-\mathbf{k}). \tag{A.13}$$

When the paired particles are in their singlet state (i.e. odd under exchange), the effective pairing potential $\hat{\Delta}$ is an even function in k-space

$$\hat{\Delta}(\mathbf{k}) = -\hat{\Delta}^T(\mathbf{k}) \tag{A.14}$$

which means that $\hat{\Delta}(\mathbf{k})$ is an antisymmetric matrix. This matrix can be written by introducing a single even function $\psi(\mathbf{k})$

$$\hat{\Delta}(\mathbf{k}) = i\hat{\sigma}_y \psi(\mathbf{k}) = \begin{bmatrix} 0 & \psi(\mathbf{k}) \\ -\psi(\mathbf{k}) & 0 \end{bmatrix}. \tag{A.15}$$

For triplet paring (i.e. even under exchange), the effective pair potential is an odd function in k-space, hence $\hat{\Delta}$ is symmetric and can be characterized by a vectorial

function $\mathbf{d}(\mathbf{k})$ which is odd in k.

$$\hat{\Delta}(\mathbf{k}) = i(\mathbf{d}(\mathbf{k}).\hat{\sigma})\hat{\sigma}_y = \begin{bmatrix} -d_x(\mathbf{k}) + id_y(\mathbf{k}) & d_z(\mathbf{k}) \\ d_z(\mathbf{k}) & d_x(\mathbf{k}) + id_y(\mathbf{k}) \end{bmatrix} \quad (A.16)$$

The solution to the transformation matrix $U_k^\dagger$ can be divided into two categories based on whether $\hat{\Delta}$ matrices are unitary or non-unitary. For singlet pairing $\hat{\Delta}$ is always unitary

$$\hat{\Delta}\hat{\Delta}^\dagger \propto \sigma_0. \quad (A.17)$$

On the other hand, the triplet $\hat{\Delta}$ matrix can either be unitary or non-unitary depending on the quantity $\mathbf{q}$,

$$\hat{\Delta}\hat{\Delta}^\dagger := |\mathbf{d}|^2 + \mathbf{q}.\hat{\sigma}$$
$$\mathbf{q} = i(\mathbf{d} \times \mathbf{d}^*) \quad (A.18)$$

This state is unitary if $\mathbf{q}$ vanishes, otherwise it is non-unitary. The solution to Equation (A.11) for the unitary case is given by

$$\hat{u_\mathbf{k}} = \frac{[E_\mathbf{k} + \varepsilon(\mathbf{k})]\sigma_0}{\{[E_\mathbf{k} + \varepsilon(\mathbf{k})]^2 + \frac{1}{2}tr\hat{\Delta}\hat{\Delta}^\dagger(\mathbf{k})\}^{1/2}}$$
$$\hat{v_\mathbf{k}} = \frac{-\hat{\Delta}(\mathbf{k})}{\{[E_\mathbf{k} + \varepsilon(\mathbf{k})]^2 + \frac{1}{2}tr\hat{\Delta}\hat{\Delta}^\dagger(\mathbf{k})\}^{1/2}} \quad (A.19)$$

where the energy spectrum of the elementary excitations is defined by

$$E_{\mathbf{k}+} = E_{\mathbf{k}-} = E_\mathbf{k} = [\varepsilon^2(\mathbf{k}) + \frac{1}{2}tr\hat{\Delta}\hat{\Delta}^\dagger(\mathbf{k})]^{1/2} \quad (A.20)$$

For non-unitary $\hat{\Delta}$, these solutions are more complicated. The $\hat{u_k}$ matrix is given by

$$
\hat{u_k} = \mathcal{Q}\left[\left(\frac{E_{\mathbf{k}+} + \varepsilon(\mathbf{k})}{E_{\mathbf{k}+}}\right)^{1/2} (|\mathbf{q}|\hat{\sigma_0} + \mathbf{q}.\hat{\sigma})(\hat{\sigma_0} + \hat{\sigma_z}) \right.
$$
$$
\left. + \left(\frac{E_{\mathbf{k}-} + \varepsilon(\mathbf{k})}{E_{\mathbf{k}-}}\right)^{1/2} (|\mathbf{q}|\hat{\sigma_0} - \mathbf{q}.\hat{\sigma})(\hat{\sigma_0} - \hat{\sigma_z}) \right]
$$

(A.21)

and the $\hat{v_k}$ matrix can be written as

$$
\hat{v_k} = -i\mathcal{Q}\left[\frac{1}{\sqrt{E_{\mathbf{k}+}[E_{\mathbf{k}+} + \varepsilon(\mathbf{k})]}}[\ \mathbf{q}|\mathbf{d} - i(\mathbf{d}\times\mathbf{q})].\hat{\sigma}\hat{\sigma_y}(\hat{\sigma_0} + \hat{\sigma_z}) \right.
$$
$$
\left. + \frac{1}{\sqrt{E_{\mathbf{k}-}[E_{\mathbf{k}-} + \varepsilon(\mathbf{k})]}}[|\mathbf{q}|\mathbf{d} + i(\mathbf{d}\times\mathbf{q})].\hat{\sigma}\hat{\sigma_y}(\hat{\sigma_0} - \hat{\sigma_z}) \right]
$$

(A.22)

with the following definitions

$$
\mathcal{Q}^{-2} = 4|\mathbf{q}|(|\mathbf{q}| + q_z)
$$
$$
E_{\mathbf{k}\pm} = \sqrt{\varepsilon(\mathbf{k})^2 + |\mathbf{d}(\mathbf{k})|^2 \pm |\mathbf{q}(\mathbf{k})|}
$$

(A.23)

In this work, the U_k matrix is used to find the quantum states of the quasi-particles at the interface of a normal-metal/superconductor junction. Then one can find the conduction coefficients from these quantum states by employing the BdG equations and appropriate boundary conditions.

Appendix B

Conductance coefficients calculations

Assuming injected electrons with $k_z > 0$ in the normal-metal side of the junction, the reflected particles can be either electrons or holes with $k_z < 0$. The spin of these particles can posses two orientations, up and down. Then the normal-side Hamiltonian is given by

$$H = \begin{pmatrix} \epsilon & 0 & 0 & 0 \\ 0 & \epsilon & 0 & 0 \\ 0 & 0 & -\epsilon & 0 \\ 0 & 0 & 0 & -\epsilon \end{pmatrix} \tag{B.1}$$

where ϵ is measured with respect to the Fermi surface. The trial solution to the eigenvalue problem for this Hamiltonian are plane waves for each component of the spinor,

$$\psi(\mathbf{r}) = \exp(i\mathbf{k}.\mathbf{r}) \tag{B.2}$$

where appropriate $\mathbf{k}$ vector should be used for various excitations (holes and electrons). In the superconductor side, the Hamiltonian is given by (see Appendix A)

$$H = \begin{pmatrix} \epsilon(\mathbf{k})\sigma_0 & \Delta(\mathbf{k}) \\ \Delta^*(-\mathbf{k}) & -\epsilon(\mathbf{k})\sigma_0 \end{pmatrix}. \tag{B.3}$$

This Hamiltonian can be diagonalized by using the appropriate unitary transformation $U_{\mathbf{k}}$,

$$\tilde{E}_{\mathbf{k}} = \begin{pmatrix} E_{\mathbf{k}+} & 0 & 0 & 0 \\ 0 & E_{\mathbf{k}-} & 0 & 0 \\ 0 & 0 & -E_{-\mathbf{k}+} & 0 \\ 0 & 0 & 0 & -E_{-\mathbf{k}-} \end{pmatrix} = U_{\mathbf{k}}^\dagger H U_{\mathbf{k}} \tag{B.4}$$

The eigenstates of this Hamiltonian are the basis column vectors,

$$|\hat{E}_{\mathbf{k}+}\rangle = \begin{pmatrix} 1 \\ 0 \\ 0 \\ 0 \end{pmatrix} \tag{B.5}$$

$$|\hat{E}_{\mathbf{k}-}\rangle = \begin{pmatrix} 0 \\ 1 \\ 0 \\ 0 \end{pmatrix} \tag{B.6}$$

$$|\hat{E}_{-\mathbf{k}+}\rangle = \begin{pmatrix} 0 \\ 0 \\ 1 \\ 0 \end{pmatrix} \tag{B.7}$$

$$|\hat{E}_{-\mathbf{k}-}\rangle = \begin{pmatrix} 0 \\ 0 \\ 0 \\ 1 \end{pmatrix} \tag{B.8}$$

Since $\hat{E}_{\mathbf{k}} = U_{\mathbf{k}}^{\dagger} H U_{\mathbf{k}}$, the eigenstates of H are given by $U|\psi\rangle$ where $|\psi\rangle$ is one of the matrices in Equation (B.4). Therefore, the physical basis eigenstates are written as

$$\psi_{\mathbf{k}+} = \begin{pmatrix} U_{11} \\ U_{21} \\ U_{31} \\ U_{41} \end{pmatrix} \tag{B.9}$$

$$\psi_{\mathbf{k}-} = \begin{pmatrix} U_{12} \\ U_{22} \\ U_{32} \\ U_{42} \end{pmatrix} \tag{B.10}$$

$$\psi_{-\mathbf{k}+} = \begin{pmatrix} U_{13} \\ U_{23} \\ U_{33} \\ U_{43} \end{pmatrix} \tag{B.11}$$

$$\psi_{-\mathbf{k}-} = \begin{pmatrix} U_{14} \\ U_{24} \\ U_{34} \\ U_{44} \end{pmatrix} \tag{B.12}$$

with eigenvalues $E_{\mathbf{k}+}$, $E_{\mathbf{k}-}$, $-E_{-\mathbf{k}+}$ and $-E_{-\mathbf{k}-}$ respectively. U_{ij} are the components of the transformation matrix which are given by (see Appendix A

$$U_k = \begin{bmatrix} \hat{u}_k & \hat{v}_k \\ \hat{v}_{-k}^* & \hat{u}_{-k}^* \end{bmatrix}. \tag{B.13}$$

The aforementioned states correspond to negative and positive energy electrons. There-

fore, the negative energy electron states need to be re-written as positive energy holes. In the hole picture, the Hamiltonian in the normal-metal side is

$$H = \begin{pmatrix} -\epsilon & 0 & 0 & 0 \\ 0 & -\epsilon & 0 & 0 \\ 0 & 0 & \epsilon & 0 \\ 0 & 0 & 0 & \epsilon \end{pmatrix} \tag{B.14}$$

while in the superconducting side this Hamiltonian takes the form

$$H = \begin{pmatrix} -\epsilon(\mathbf{k})\sigma_0 & \Delta(\mathbf{k}) \\ -\Delta^*(-\mathbf{k}) & \epsilon(\mathbf{k})\sigma_0 \end{pmatrix}. \tag{B.15}$$

Similar to the electron picture, the quasi-particle states are described in terms of the components of the transformation matrix U_k which in the hole picture is given by

$$U_k = \begin{bmatrix} \hat{u_k} & -\hat{v_k} \\ -v^*_{-k} & u^*_{-k} \end{bmatrix}. \tag{B.16}$$

These eigenstates (positive energy electrons and positive energy holes) can be used in the solution of the BdG equations at the interface of normal-metal/insulator/PrOs$_4$Sb$_{12}$ junctions. The conductance coefficients are calculated by using the following Mathematica code:

This code calculates conductance coefficients of a junction for spin-up electron injection

b11 = spin-up electron

b12 = spin-down electron

a11 = spin-up hole

a12 = spin-down hole

Unm = components of the transformation matrix for positive energy electrons and holes

All the wave vectors in the problem are already fixed to k_F

Remove["Global`*"]

Normal - metal (N) side wave function

uN1[x_]:=Exp[ICos[θ]x] + b011Exp[$-I$Cos[θ]x];

uN2[x_]:=b012Exp[$-I$Cos[θ]x];

vN1[x_]:=a011Exp[ICos[θ]x];

vN2[x_]:=a012Exp[ICos[θ]x];

Superconductor (S) side wave function

uS1[x_]:=c01Exp[ICos[θ]x]U11 + c02Exp[ICos[θ]x]U12 + d01Exp[$-I$Cos[θ]x]U13+ d02Exp[$-I$Cos[θ]x]U14;

uS2[x_]:=c01Exp[ICos[θ]x]U21 + c02Exp[ICos[θ]x]U22 + d01Exp[$-I$Cos[θ]x]U23+ d02Exp[$-I$Cos[θ]x]U24;

vS1[x_]:=c01Exp[ICos[θ]x]U31 + c02Exp[ICos[θ]x]U32 + d01Exp[$-I$Cos[θ]x]U33+ d02Exp[$-I$Cos[θ]x]U34;

vS2[x_]:=c01Exp[ICos[θ]x]U41 + c02Exp[ICos[θ]x]U42 + d01Exp[$-I$Cos[θ]x]U43+ d02Exp[$-I$Cos[θ]x]U44;

First derivatives – N side

uN1f[x_] = ∂_xuN1[x];

uN2f[x_] = ∂_xuN2[x];

vN1f[x_] = ∂_xvN1[x];

vN2f[x_] = ∂_xvN2[x];

First derivatives – S side

uS1f[x_] = ∂_xuS1[x];

```
uS2f[x_] = ∂ₓuS2[x];
```

$$uS2f[x\_] = \partial_x uS2[x];$$

$$vS1f[x\_] = \partial_x vS1[x];$$

$$vS2f[x\_] = \partial_x vS2[x];$$

Boundary conditions

$$eqn3 = \{uS1[0] - uN1[0] == 0, uS2[0] - uN2[0] == 0, vS1[0] - vN1[0] == 0,$$

$$vS2[0] - vN2[0] == 0, uS1f[0] - uN1f[0] == 2ZuN1[0], uS2f[0] - uN2f[0] == 2ZuN2[0],$$

$$vS1f[0] - vN1f[0] == 2ZvN1[0], vS2f[0] - vN2f[0] == 2ZvN2[0]\};$$

Finding conductance coefficients

$$sol3 = Solve[eqn3, \{a011, a012, b011, b012, c01, c02, d01, d02\}];$$

$$a11 = a011/.sol3;$$

$$a12 = a012/.sol3;$$

$$b11 = b011/.sol3;$$

$$b12 = b012/.sol3;$$

$$c1 = c01/.sol3;$$

$$c2 = c02/.sol3;$$

$$d1 = d01/.sol3;$$

$$d2 = d02/.sol3;$$

Conductance coefficients

$$a11 = a11[[1]];$$

$$a12 = a12[[1]];$$

$$b11 = b11[[1]];$$

$$b12 = b12[[1]];$$

This code calculates conductance spectrum for a singlet superconductor

Remove["Global`*"]

Defining gap function

$\delta[\theta\_,\phi\_]:=\mathrm{Cos}[\theta]\wedge 2 - .5\mathrm{Sin}[\theta]\wedge 2 + I.5\mathrm{Sqrt}[3]\mathrm{Sin}[\theta]\wedge 2\mathrm{Cos}[2\phi]$

Defining U matrix components

$\mathrm{up} = \sqrt{((y + \sqrt{(y\wedge 2 - \mathrm{Abs}[\delta[\theta,\phi]]\wedge 2)})/(2y))};$

$\mathrm{vp} = \sqrt{((y - \sqrt{(y\wedge 2 - \mathrm{Abs}[\delta[\theta,\phi]]\wedge 2)})/(2y))};$

$\mathrm{um} = \sqrt{((y + \sqrt{(y\wedge 2 - \mathrm{Abs}[\delta[\theta,\phi + \pi]]\wedge 2)})/(2y))};$

$\mathrm{vm} = \sqrt{((y - \sqrt{(y\wedge 2 - \mathrm{Abs}[\delta[\theta,\phi + \pi]]\wedge 2)})/(2y))};$

$\mathrm{phasep} = \delta[\theta,\phi]/\mathrm{Abs}[\delta[\theta,\phi]];$

$\mathrm{phasem} = \delta[\theta,\phi + \pi]/\mathrm{Abs}[\delta[\theta,\phi + \pi]];$

$\mathrm{U11} = \mathrm{up};$

$\mathrm{U12} = \mathrm{vm};$

$\mathrm{U21} = \mathrm{vpphasep};$

$\mathrm{U22} = \mathrm{umphasem};$

Wave functions and their first derivatives

$\mathrm{uN1}[\mathrm{x\_}]:=\mathrm{Exp}[I\mathrm{Cos}[\theta]x] + \mathrm{b0Exp}[-I\mathrm{Cos}[\theta]x];$

$\mathrm{vN2}[\mathrm{x\_}]:=\mathrm{a0Exp}[I\mathrm{Cos}[\theta]x];$

$\mathrm{uS1}[\mathrm{x\_}]:=\mathrm{c0Exp}[I\mathrm{Cos}[\theta]x]\ \mathrm{U11}+$

$\mathrm{d0Exp}[-I\mathrm{Cos}[\theta]x]\ \mathrm{U12};$

$\mathrm{vS2}[\mathrm{x\_}]:=\mathrm{c0Exp}[I\mathrm{Cos}[\theta]x]\ \mathrm{U21}+$

$\mathrm{d0Exp}[-I\mathrm{Cos}[\theta]x]\ \mathrm{U22};$

$\mathrm{uN1f}[\mathrm{x\_}] = \partial_x\mathrm{uN1}[x];$

$\mathrm{vN2f}[\mathrm{x\_}] = \partial_x\mathrm{vN2}[x];$

$\mathrm{uS1f}[\mathrm{x\_}] = \partial_x\mathrm{uS1}[x];$

$\mathrm{vS2f}[\mathrm{x\_}] = \partial_x\mathrm{vS2}[x];$

Boundary conditions

eqn3 = {

  uS1[0] − uN1[0]==0,

  vS2[0] − vN2[0]==0,

  uS1f[0] − uN1f[0]== 2Z uN1[0],

  vS2f[0] − vN2f[0]==2Z vN2[0]};

Conductance coefficients

sol3 = Solve[eqn3, {a0, b0, c0, d0}];

a = a0/.sol3;

b = b0/.sol3;

c = c0/.sol3;

d = d0/.sol3;

a = a[[1]];

b = b[[1]];

Angle-resolved conductance

sigmaS[Z_, θ_, ϕ_, y_] = 1 + Abs[a]^2 − Abs[b]^2;

f[Z_, y_]:=NIntegrate[Sin[θ]sigmaS[Z, θ, ϕ, y], {θ, 0, π/2}, {ϕ, 0, 2π}]

Normal conductance

sigmaN[Z_, θ_] = Cos[θ]^2/(Z^2 + Cos[θ]^2);

n[Z_]:=NIntegrate[Sin[θ]sigmaN[Z, θ], {θ, 0, π/2}, {ϕ, 0, 2π}]

Normalized conductance for various Z values

r0 = Table[{y, f[.000000001, y]/n[0.000000001]}, {y, 0.00001, 2, 0.02}];

r1 = Table[{y, f[.2, y]/n[0.2]}, {y, 0.00001, 2, 0.02}];

r2 = Table[{$y, f[.5, y]/n[0.5]$}, {$y, 0.00001, 2, 0.02$}];

r3 = Table[{$y, f[.8, y]/n[0.8]$}, {$y, 0.00001, 2, 0.02$}];

Bibliography

[1] J. Bardeen, L. N. Cooper, and J. R. Schrieffer, *Phys. Rev.* **106**, 162–164 (1957).

[2] M. Sigrist and K. Ueda, *Rev. Mod. Phys.* **63**, 239 (1991).

[3] I. A. Sergienko and S. H. Curnoe, *Phys. Rev.* B **70**, 144522 (2004).

[4] E.D. Bauer *et al.*, *Phys. Rev.* B **46**, 100506(R) (2002).

[5] M.B. Maple *et al.*, *J. Phys. Soc. Jpn.* **71**, Sup. 23 (2002).

[6] R. Vollmer *et al.*, *Phys. Rev. Lett.* **90**, 057001 (2003).

[7] T. Tayama *et al.*, *J. Phys. Soc. Jpn.* **72**, 1516 (2003).

[8] E.E.M. Chia *et al.*, *Phys. Rev. Lett.* **91**, 247003 (2003).

[9] N.A. Frederick *et al.*, *J. Low Temp. Phys.* **147**, 321 (2007).

[10] K. Izawa *et al.*, *Phys. Rev. Lett.* **90**, 117001 (2003).

[11] M.B. Maple *et al.*, *J. Super. Nov. Mag.* **19**, 299 (2006).

[12] R. Joynt and L. Taillefer, *Rev. Mod. Phys.* **74**, 235 (2002).

[13] G. Seyfarth *et al.*, *Phys. Rev. Lett.* **97**, 236403 (2006).

[14] R.W. Hill *et al.*, *Phys. Rev. Lett.* **101**, 237005 (2008).

[15] G. Deutscher, *Rev. Mod. Phys.* **77**. 109 (2005).

[16] A. M. Duif, A. G. M. Jansen and P. Wyder, *J. Phys.: Condens. Matter.* **1**, 3157 (1989).

[17] A. Andreev, *Zh. Eksp. Teor. Fiz.* **46**, 1823 (1964).

[18] Y. V. Sharvin, *Zh. Eksp. Teor. Fiz.* **48**, 984 (1965).

[19] de Gennes, P., 1966, *Superconductivity of Metals and Alloys* (Benjamin, New York), p. 137.

[20] A.M. Duif, A.G.M. Jansen and P. Wyder, *J. Phys.:Condens. Matter* **1**, 3157–89 (1989).

[21] G.E. Blonder, M. Tinkham and T.M. Klapwijk, *Phys. Rev.* B **25**, 4515 (1982).

[22] S. Kashiwaya and Y. Tanaka, *Rep. Prog. Phys.* **63**, 1641 (2000).

[23] R. Landauer, *Phil. Mag.* **21** 863, (1970).

[24] D. Daghero and R. S. Gonnelli, *Supercond. Sci. Technol.* **23**, 043001 (2010).

[25] C. Bruder, *Phys. Rev.* B **41**, 4017 (1990).

[26] S. Kashiwaya, Y. Tanaka, M. Koyanagi and K. Kajimura, *Phys. Rev.* B **53**, 2667 (1996).

[27] M. Yamashiro *et al.*, *Physica* C **293**, 239 (1997).

[28] C. R. Hu, *Phys. Rev. Lett.* **72**, 1526 (1994).

[29] C. Honerkamp and M. Sigrist, *J. Low Temp. Phys.* **111**, 895 (1998).

[30] M. Yamashiro *et al.*, *J. Phys. Soc. Jpn.* **67**, 3224 (1998).

[31] J. Linder and A. Sudbø, *Phys. Rev.* B **75**, 134509 (2007).

[32] M. Yamashiro and Y. Tanaka, *Phys. Rev.* B **56**, 7847 (1997).

[33] M.B. Maple *et al.*, *J. Super. Nov. Mag.* **19**, 299 (2006).

[34] H. Sugawara *et al.*, *Phys. Rev.* B **66**, 220504 (2002).

[35] D.E. MacLaughlin *et al.*, *Physica* B **403**, 1132 (2008).

[36] L. Shu *et al.*, *Phys. Rev.* B **79**, 174511 (2009).

[37] G. Seyfarth *et al.*, *Phys. Rev. Lett.* **97**, 236403 (2006).

[38] R.W. Hill *et al.*, *Phys. Rev. Lett.* **101**, 237005 (2008).

[39] L. D. Landau, 1965, *Collected papers* (Oxford: Pergamon Press), p. 137.

[40] S. H. Curnoe, unpublished work.

[41] C. S. Turel *et al.*, arXiv:1110.5104v1 [cond-mat.supr-con] (2011).

[42] C. Turel, *Probing Exotic Superconducting Order Parameter Symmetry Using Point-Contact Andreev Reflection* ⟨Ph.D. Thesis⟩, University of Toronto (2009).